Agricultural and Forest Meteorology 301-302 (2021) 108337

Contents lists available at ScienceDirect

Agricultural and Forest Meteorology

journal homepage: www.elsevier.com/locate/agrformet

Disaggregating the effects of nitrogen addition on gross primary production in a boreal Scots pine forest

Xianglin Tian [a,*], Francesco Minunno [a], Pauliina Schiestl-Aalto [a,b], Jinshu Chi [b], Peng Zhao [b], Matthias Peichl [b], John Marshall [b], Torgny Näsholm [b], Hyungwoo Lim [b], Mikko Peltoniemi [c], Sune Linder [d], Annikki Mäkelä [a]

[a] Department of Forest Sciences, University of Helsinki, P.O. Box 27, Helsinki FI-00014, Finland
[b] Department of Forest Ecology and Management, Swedish University of Agricultural Sciences (SLU), SE-901 83 Umeå, Sweden
[c] Natural Resources Institute Finland (Luke), Latokartanonkaari 9, Helsinki FI-00790, Finland
[d] Southern Swedish Forest Research Centre, SLU, P.O. Box 49, SE-230 53 Alnarp, Sweden

ARTICLE INFO

Keywords:
Nitrogen addition
Gross primary production
Light use efficiency
Inverse modelling
Environmental restrictions
boreal forests

ABSTRACT

Adding nitrogen to boreal forest ecosystems commonly increases gross primary production (GPP). The effect of nitrogen addition on ecosystem GPP is convoluted due to the impacts of and interactions among leaf scale photosynthetic productivity, canopy structure, site fertility, and environmental constraints. We used a unique controlled nitrogen fertilisation experiment combined with eddy covariance measurements and the calibration of a LUE-based (light use efficiency) photosynthetic production model in order to reveal differences in photosynthetic capacity due to nitrogen addition.A systematically designed soil moisture survey was conducted to characterise the within-site spatial heterogeneity and validate the difference of water stress between fertilised and control sites. The canopy photosynthetic light responses and environmental constraints were evaluated using an inverse modelling approach. We found that nitrogen fertilisation elevated ecosystem GPP by 24% according to model simulations. This was caused by increases in ecosystem light interception (through an increase in leaf area index (LAI)) and LUE by 7% and 17%, respectively. Nitrogen addition increased canopy potential LUE for both low and high photosynthetic photon flux density (PPFD) conditions. The calculations of leaf area and light interception indicated that the understorey vegetation contributed 9% of ecosystem GPP in the fertilised site and 7% in the control site when assuming a same LUE for trees and shrubs. The constraint arising from atmospheric water demand, rather than soil water stress, was the dominating control of the intra- and inter-annual GPP variations. The uncertainty propagated from soil moisture data is negligible for GPP predictions, but influential in the inference on the severity of the drought. This study demonstrates the combination of the controlled field experiment with the inverse modelling approach provides a powerful tool to quantitatively describe and disaggregate N addition effects on forest ecosystem GPP.

1. Introduction

Despite the large amount of organic nitrogen stored in boreal soils, the productivity of boreal forest is still limited by available soluble nitrogen due to its slow decomposition rate (Nömmik and Vahtras, 1982; Tamm, 1991; Vitousek and Howarth, 1991; Rustad et al., 2001). Nitrogen availability effects on forest photosynthesis have been quantified at the leaf level using gas-exchange measurements (Tang et al., 1999; Palmroth et al., 2014), as well as the stand level using eddy covariance (EC) measurements (Magnani et al., 2007; Peltoniemi et al., 2012a). Nitrogen addition significantly promotes stem growth and needle nitrogen concentration of coniferous forests (Nohrstedt, 2001; From et al., 2015). Numerous leaf level studies have shown that increased leaf nitrogen concentration will promote leaf photosynthetic capacity (Field and Mooney, 1986; Evans, 1989; Reich et al., 1995, 1997; Wright et al., 2004).

Stand level photosynthetic responses to nitrogen addition are complex considering that the availability of light and water for single leaves varies within the canopy (Palmroth et al., 2014; Tarvainen et al., 2016) as a result of different leaf morphology, structure, orientation and

* Corresponding author.
E-mail address: xianglin.tian@helsinki.fi (X. Tian).

https://doi.org/10.1016/j.agrformet.2021.108337
Received 9 October 2020; Received in revised form 14 January 2021; Accepted 18 January 2021
Available online 6 February 2021

nitrogen content per area change throughout the canopy profile (Ellsworth and Reich, 1993; Stenberg et al., 1995; Kull and Niinemets, 1998). Previous studies indicated that canopies optimize their structure for the optimal co-allocation of nitrogen and water supply (e.g. Peltoniemi et al., 2012b). However, experiments at stand level have not always been able to control the environmental variation adequately. Foliar nitrogen content may not be able to explain the variation in light-saturated CO_2 exchange rate because of the complexity of plant hydraulic properties and within-site variation in water stress (Palmroth et al., 2014). The effects of nitrogen-addition on shoot and canopy scale might further be blurred by deficiency of other nutrients and arginine synthesis (Tarvainen et al., 2016). Thus, our current understanding of nitrogen availability effects on gross primary production (GPP) at the stand level is incomplete.

The stand-level interactions between photosynthesis and environmental constraints can be described in terms of ecosystem light use efficiency (LUE) (e.g. Mäkelä et al., 2008; Yuan et al., 2014). Defined as gross primary production divided by absorbed PPFD (photosynthetic photon flux density), LUE is a crucial parameter to explain the variations of forest production (Landsberg and Sands, 2011). Biomes differ significantly with respect to the maximum of daily actual LUE (Turner et al., 2003). Using a selection of EC sites, Kergoat et al. (2008) found that mean annual temperature and foliar nitrogen explained 80% of variance in maximum daily LUE in temporal and boreal ecosystems, and that LUE at high PPFD was nitrogen dependent. Likewise, Peltoniemi et al. (2012a) found that the ecosystem potential (theoretical maximum) LUE was positively correlated with the canopy nitrogen concentration at all light levels, implying that nitrogen affects LUE also at low PPFD. When using datasets of large geographical scales, the linkage between foliar nitrogen and canopy LUE might be masked and marginalised by the spatial variation of environmental conditions (Schwalm et al., 2006).

Enhanced nitrogen availability due to atmospheric deposition or fertilisation might affect the contributions of overstorey and understorey to ecosystem GPP because of their contrasting responses to changes in shoot structure, canopy openness, and light interception (Stenberg et al., 1999). However, this effect has not been explicitly quantified in previous studies because of the confounding interactions between varying plant traits, environmental conditions and site fertility. In boreal forests, the contribution of the ground vegetation to ecosystem CO_2 exchange and photosynthetic production has been measured for various sites and conditions, mainly using chamber or EC methods (eg. Goulden and Crill, 1997; Morén and Lindroth, 2000; Misson et al., 2007; Kulmala et al. 2009; Kulmala et al. 2011; Paul-Limoges et al., 2017). Goulden and Crill (1997) estimated that moss photosynthesis accounted for 10 – 50% of the entire forest gross CO_2 uptake based on simultaneous measurements from chamber and EC in black spruce forests in central Manitoba, Canada. With EC measurements above and below canopy, Misson et al. (2007) showed that understorey GPP was up to 39% of the ecosystem GPP, with an average of 14% across the boreal and temperate forests.

Previous experiments have found that nitrogen addition decreases the ratio of root-to-leaf area, saturated hydraulic conductivity of fine roots, and the leaf-specific conductivity (Ewers et al., 2000; Ewers et al., 2001). Furthermore, tree growth measurements (Lim et al., 2015) and carbon isotope analysis (Betson et al, 2007) suggest that nitrogen-addition increases the susceptibility of stem wood production in boreal Scots pine forests to drought. Thus, nitrogen addition might render stand GPP more drought-sensitive. However, natural drought can be an elusive phenomenon and thus difficult to quantify its occurrence, severity, and impacts on ecosystem GPP. Soil water availability is commonly used to characterize the ecosystem moisture stress (Rodrigues-Itube and Porporato, 2004; Beier et al, 2012), and to assess drought indicators in representing summer drought in boreal forest (Gao et al., 2016). Nevertheless, the atmospheric demand for water also affects photosynthetic productivity since plants close their stomata at high vapour pressure deficit (VPD) conditions to avoid excessive water loss through transpiration (Cowan and Farquhar, 1977; Oren et al., 1999; McAdam and Brodribb, 2015). Atmospheric demand has been reported to limit surface conductance and evapotranspiration to a greater extent than soil moisture in many mesic forests (Novick et al., 2016). Separating soil water and VPD effects from those of nitrogen fertilisation is even more important for evaluation of the subsequent shifts in carbohydrate partitioning from belowground to favour aboveground biomass production (Linder and Axelsson, 1982; Haynes and Gower, 1995; Nilsson and Wallander, 2003).

Table 1
Site summary. The values of leaf area index (LAI) are projected-area based (m^2 m^{-2}).

	Fertilised	Control	Reference
Site ID	Ros2	Ros3	
Latitude/longitude	64°10'N 19°45'E (each stand ~16 ha and ~2 km apart)		
Mean annual air temperature	3.0 °C (2014-2018)		This study (Measurement)
Mean annual precipitation	553 mm (2014-2018)		This study (Measurement)
LAI of trees	3.4 (2011)	2.6 (2011)	Lim et al., 2015
LAI of trees	2.9 (2018)	2.8 (2018)	This study (Measurement)
LAI of ground vegetation	1.0	0.52	This study (Section 2.3)
Field capacity	25.6%	16.8%	This study (Section 2.6)
Wilting point	5.9%	5.9%	Duursma et al., 2008

A controlled experiment minimises the between-treatment variation in environmental constraints that regulate photosynthesis, other than nitrogen availability. Thus, the difference in photosynthetic capacity between stands can be attributed to nitrogen addition. A controlled nitrogen fertilisation experiment on mature *Pinus sylvestris* was established in northern Sweden, Rosinedalsheden experimental forests in 2005. This unique experiment is ideally suited for investigating the effect of nitrogen addition on forest productivity. Inter-annual variability of precipitation has been found to constrain the growth response effectively when nitrogen limitation is alleviated according to destructive tree sampling from the experimental stands (Lim et al., 2015). However, increased needle nitrogen contents have not been found to improve shoot photosynthetic performance based on chamber measurements (Tarvainen et al., 2016). Although both EC and chamber measurements can generally quantify the nitrogen effect on forest GPP, flux data alone cannot distinguish between contributing effects from stand structural changes and variations in environmental conditions. Meanwhile, unexplained daily variation and substantial measurement uncertainty tend to blur most quantitative interpretations about the nitrogen addition effect.

This study is based on the unique combination of EC measurements from the Rosinedalsheden nitrogen fertilisation experimental sites and a state-of-the-art LUE-based, daily time-step, photosynthetic production model. Our objectives were: i) to quantify how the nitrogen addition affects ecosystem GPP and daily photosynthetic light responses of the canopy, ii) to partition the changes in GPP into contributions from changes in light interception and LUE, iii) to partition the changes in GPP into tree canopy and understorey contributions and iv) to assess the impact of various environmental stresses on intra- and inter-annual GPP variation. We hypothesized that i) nitrogen addition increases LUE at all light levels at daily and ecosystem scales, ii) the effect of higher light interception due to nitrogen addition dominates the increases of ecosystem GPP, iii) increased shading from canopy of trees leads to lower GPP of ground vegetationand, iv) nitrogen addition renders stand GPP more drought-sensitive.

2. Materials and methods

2.1. Fertilisation experiments

The study was conducted in the Rosinedalsheden experimental forest (Table 1). The forest consists of naturally generated 100-year-old Scots pines (*Pinus sylvestris* L.). This stand was regenerated with seed trees in 1920-1925, pre-commercially thinned in 1955, and respectively thinned in 1976 and 1993. The field layer is dominated by bilberry (*Vaccinium myrtillus* L.) and lingonberry (*Vaccinium vitis-idaea* L.). The soil is formed on fine sandy and silty glacial outwash sediments. The experimental stands share similar soil texture, and deep sandy sediment with 2–5 cm soil organic layer (Mellander et al., 2005). The annual total atmospheric reactive nitrogen deposition (sum of wet and dry deposition) to coniferous forests in the north of Sweden during the period 2004-2013 is approximately 1.9 kg N ha^{-1} yr^{-1} (Phil-Karlsson et al., 2009; Andersson et al., 2018). The experiment was laid out in the summer of 2005 and annual nitrogen fertilisation started in 2006 over a 16-ha area within this forest. The addition of nitrogen for the experimental site was 100 kg N ha^{-1} yr^{-1} from 2006 to 2011, and then reduced to 50 kg N ha^{-1} yr^{-1} from 2012 onwards (Lim et al., 2015). Skog-Can fertilizer (Yara, Sweden), containing N (27%), Ca (5%), Mg (2.4%), and B (0.2%), was applied in mid-June each year (Lim et al., 2015). The amount N is equally from NH_4^+ and NO_3^-, which means that the mass of NH_4NO_3 accounts for ~77% of total fertilizer mass. No treatment was performed for the control site located ~2 km away from the fertilised area. Mean annual temperature and precipitation from 1981 to 2013, recorded at Svartberget climate station 8 km from experiment site, were respectively 1.8 °C and 614 mm (Laudon et al., 2013).

2.2. Eddy covariance measurements

The net ecosystem exchange of CO_2 (NEE) and evapotranspiration (ET) were measured using the EC method for both fertilised and control plots. Our analysis was based on the EC data from August 2014 to December 2018. At each site, EC systems were deployed above the canopy at the height of 21.5 m. The EC systems were identical at the two sites, consisting of a Gill R3-100 (Gill Instruments Limited, Hampshire, UK) sonic anemometer for measuring the wind components and a LI-7200 (LI-COR Environmental, Lincoln, USA) gas analyser for measuring the $CO_2$and H_2O concentrations. The EC raw data were recorded at 20 Hz and processed in the EddyPro software (version 7.0.6, LI-COR Biosciences) to obtain the half-hourly averaged fluxes. Double coordinate rotation was used to align the sonic anemometer with the local wind streamlines (Wilczak et al., 2001), block averaging was used to determine the turbulent fluctuations over each 30-min averaging period (Gash and Culf, 1996), and time lags between sonic and IRGA were determined by automatic time lag optimization method. Half-hourly NEE and ET data were filtered for non-steady state or undeveloped turbulent conditions (Mauder and Foken 2004), low signal strength of EC instruments, decoupling between the below- and above-canopy air masses (Jocher et al. 2017, 2018), and statistical outliers (Papale et al. 2006). After the quality control and filtering, 45 ± 28 (SD) % and 40 ± 26 (SD) % of all half-hourly NEE and ET values remained each day. Gaps in the 30-min NEE and ET data were filled using the Max-Plank online gap-filling tool (Wutzler et al. 2018). GPP was separated from NEE using nighttime-based partitioning method (Reichstein et al., 2005). Eventually, the half-hourly GPPand ET were aggregated into daily sums. A quality flag (QC, quality control) varying between 0-1 was assigned for each daily record, indicating percentage of measured half-hourly data used to calculate daily value. Only the daily GPP values from days on which the quality flag was greater than 0.5 were used in calculations of actual LUE (section 2.4) and calibrations of the potential LUE and PRELES (section 2.5&2.6). Meanwhile, the model cross-validation (section 2.6) used all daily data without any minimum QC threshold, to analyse the discrepancy between daily EC-based estimates and PRELES simulations.

2.3. Light interception

Leaf area index (LAI; projected-area based) of trees was estimated by combining foliage mass and specific needle area of harvested trees from both fertilised and control sites (Lim et al., 2015). The LAI (projected-area based) of the shrubs was estimated based on published measurements of the percentage of shrub cover (Palmroth et al., 2014). An empirical relation between biomass and percentage cover in understorey vegetation of boreal coniferous forests (Muukkonen et al., 2006) was adopted to estimate the aboveground biomasses. The leaf area index of *V. myrtillus* was then estimated based on published measurements of the leaf mass fraction and leaf mass per area (Palmroth et al., 2014). *V. vitis-idaea* was randomly scattered in the stand, so the leaf area index of *V. vitis-idaea* estimated respectively for control and fertilised plots by Palmroth et al. (2014) was directly used in this analysis.

The fraction of absorbed PPFD (f_{APAR}) was estimated with accumulated leaf area according to Lambert-Beer's law:

$$f_{APAR} = \left(1 - e^{(-k_C \ L_C \ )}\right) + e^{(-k_c \ L_c \ )} \cdot \left(1 - e^{(-k_G \ L_G \ )}\right) \quad (1)$$

where k is light extinction coefficient, L is leaf area index, and the subscripts C and Grepresent, respectively, tree canopy and ground vegetation (Table 1). The extinction coefficient for tree canopy, k_C, was estimated as 0.52 (Smith et al., 1991; Mellander et al., 2005), while for ground vegetation k_G was estimated as 0.69 (Aubin et al., 2000). LAI of canopy during the peak growing season from 2014 to 2018 was set as the average of measurements in 2011 and 2018 (Table 1). The seasonal changes of LAI were simulated based on leaf growth module of CASSIA (carbon allocation sink source interaction) (Schiestl-Aalto et al., 2015).

2.4. Maximum actual LUE

Maximum actual LUE is defined as the highest actual LUE that one site could achieve, and it was here calculated directly from the observational data. The daily actual LUE was calculated as the ratio of EC derived daily GPP sums (g C m^{-2} d^{-1}) to daily absorbed/intercepted PPFD sums (mol m^{-2} d^{-1}). The maximum LUE at each site can be estimated as the upper percentile of all daily LUE, e.g. 98th percentile of high PPFD days (Kergoat et al., 2008) or 98th percentile of all days (Peltoniemi et al., 2012a). In this study, the maximum actual LUE was estimated as 95th, 97.5th and 99th percentile of daily actual LUEs. Daily LUE was calculated for those days on conditions that 1) the day is during growing season, 2) daily PPFD is greater than 5 mol m^{-2} day^{-1}, 3) value of quality flag is greater than 0.5. Estimates of LUE out of 3 standard deviations from the mean were removed after the calculation using the above three criteria. The analysis of fertilisation effects was based on the days when LUE estimates were valid from both the fertilised and the control sites.

2.5. Estimating potential LUE

The potential LUE was estimated by calibrating the ecosystem GPP and ET model estimates from PRELES (Mäkelä et al., 2008; Peltoniemi et al., 2015; Minunno et al., 2016) using site-specific meteorological and EC data. PRELES calculates the daily photosynthetic production during day k, P_k (g C m^{-2} d^{-1}), as the potential LUE parameter, β (g C mol $PPFD^{-1}$), attained under theoretically optimal conditions, multiplied by daily PPFD and a series of modifiers that describe how photosynthesis is limited by each environmental factor:

$$P_k = \beta \cdot \phi_k \cdot f_{(APAR,\ k)} \cdot f_{(L,k)} \cdot f_{(S,\ k)} \cdot f_{(E,k)} \quad (2)$$

where ϕ_k is PPFD (mol m^{-2} d^{-1}), and $f_{(APAR,\ k)}$ the fraction of ϕ_k absorbed by the canopy during day k. The f_L, f_S, and f_E, are the modifiers that describe the effects of light saturation L and the suboptimal conditions in temperature acclimation S and water stress E, respectively.

The water stress f_E is expressed as the minimum of VPD stress (f_D) and soil water stress (f_W). All modifiers are constrained between zero and one. Explanations and formulas of each modifier are given in appendix (section A1). More detailed descriptions can be found in Mäkelä et al. (2008). In calibrations, the potential LUE β was strongly correlated with a light saturation parameter γ in modifier f_L, which is

$$f_{(L,k)} = \frac{1}{\gamma \varnothing_k + 1} \tag{3}$$

Combing potential LUE parameter β with the $f_(L,k)$ modifier, $(\beta\phi_k)/(\gamma\varnothing_k + 1)$, is analogous to the common rectangular hyperbola photosynthesis model at daily level:

$$P = (qP_{\max}\ \varnothing_k)/(q\varnothing_k + P_{\max}\ ) \tag{4}$$

where $P_{\max}$ and q represent the saturated productivity and the initial slope, respectively. These two parameters can be obtained by parameters in PRELES as $P_{\max} = \beta/\gamma$ and $q = \beta$.

Because the fertilised and control sites shared the same weather drivers, the difference in model results, caused by fertility should be explained by the fractions of intercepted light (f_{APAR}) and potential LUE. We combined the EC data from fertilised and control sites, and calibrated PRELES using a hierarchical approach assuming the two sites share the same physiological parameters except the site-specific β. Considering the parameter correlation, we also implemented another hierarchical calibration that contains site-specific estimations of both β and γ while all the other parameters were shared.Besides the hierarchical calibration, a site-specific calibration was also implemented, which means that no parameter was shared, and model was calibrated independently for each site. The hierarchical calibration has been reported to be more reliable in parameter interpretations and model extrapolations (Tian et al. 2020). The site-specific calibration has a higher risk of overfitting, but is able to detect the difference between the two sites in environmental stresses (Section 2.7). The soil texture and evapotranspiration were also considered in PRELES. Thus, the simulation of soil water content varies between the sites even though weather drivers are shared.

2.6. Calibration and validation of PRELES

A Bayesian approach was adopted for PRELES calibration and uncertainty quantification (Minunno et al., 2016). This inverse modelling approach adjusted model parameters and the assumption of error distribution to their ability to reproduce stand-level field observations (i.e. EC measurements in this study). Random measurement errors are often represented by the independent Gaussian distributions in model calibrations. However, this assumption makes the parametrization easily affected by outliers in the dataset (Sivia and Skilling, 2006). The calibration of PRELES adopted a more peaked but also more heavy-tailed distribution, the double-exponential (Laplace) distribution, in order to suppress the effect of measured outliers. The likelihood function used in the calibration was:

$$p(\boldsymbol{Y}\boldsymbol{\theta}) = p(\boldsymbol{\varepsilon} = \boldsymbol{Y} - \boldsymbol{M}(\boldsymbol{\theta})) = \prod_{j=1}^{3}\prod_{i=1}^{N_j} \frac{1}{2} Exp\left(\left|\varepsilon_{j,i}\right|; \frac{1}{a_j + b_j M(\boldsymbol{\theta})_{j,i}}\right)$$
$$= \prod_{j=1}^{3}\prod_{i=1}^{N_j} \frac{1}{2\left(a_j + b_j M(\boldsymbol{\theta})_{j,i}\right)} exp\left(\frac{-\left|\varepsilon_{j,i}\right|}{a_j + b_j M(\boldsymbol{\theta})_{j,i}}\right) \tag{5}$$

where $\boldsymbol{Y}$ represents the observations, θ the parameters of the PRELES model, $p(Y|\theta)$ the probability of the data for a given parameter vector, $M(\theta)$ the outputs of the model, ε the measurement error and an unknown model structural error. $Exp(.;.)$ is the probability density function of the exponential distribution and $1/(a_j + b_j[M(\theta)]_(j,i))$ is its rate parameter. The j-subscripts index the three types of output variables, which are GPP, ET, and soil water; the i-subscripts index the data and N_j is the total number of valid observations for variable j. The rate/scale parameter of the Laplace distribution was associated with a linear model, which assumes that the uncertainty may increase with the estimate size, as we had no better knowledge of the true behaviour of the uncertainty. Parameters a and b were calibrated simultaneously with θ to approximate the relationship between rate parameters and measurement uncertainty.

Soil volumetric water content data are from two sensors per site, one at 15 cm depth and the other at 50 cm depth (Fig. A3). Soil water content was crucial for the diagnosis of water stress, but no replication was available. Thus, the average soil water content was estimated as follows:

$$\Theta_{(root,k)} = s \cdot \left[r \cdot \Theta_{(15\mathrm{cm},k)} + (1-r) \cdot \Theta_{(50\mathrm{cm},k)}\ \right] \tag{6}$$

where $\Theta_(15\mathrm{cm},k)$ and $\Theta_(50\mathrm{cm},k)$ are the observations of daily mean soil water content on day k, at depth of 15 cm and 50 cm, respectively. $\Theta_(root,k)$ is the average soil water content of the depth explored by plant roots. Parameters r, s and the field capacity (Table 1) were calibrated simultaneously with the parameters in PRELES. r is constrained between zero and one, relating with the root distribution and soil profile. s relates with the bias of the sensor. Although PRELES only simulates the average soil water storage using a simple bucket module (Section A2), predictions of soil water content at 15cm and 50cm depth can also be obtained from Eq. (6) by simultaneously fitting a linear regression between $\Theta_(15\mathrm{cm},k)$ and $\Theta_(50\mathrm{cm},k)$ using soil moisture measurement data. A sensitivity analysis of model simulations to varying biases in soil moisture data was implemented (Section A3) due to the concern about the representative of relying on only one sample location and two measurement depth for each site.

To characterise the spatial heterogeneity and validate the difference of soil moisture between fertilised and control sites, a systematically designed soil moisture survey was conducted at each site in approximately biweekly intervals from June to September 2020. Specifically, at each site, we selected 12 measurement locations every 25m along two 100m long perpendicular transects (with the flux tower located at their crossing point) and one location next to the soil profile with automated SWC measurements. At each location, soil moisture content in the upper 0-6cm layer was measured three times within a 1m radius using a handheld moisture sensor (GS3, Decagon).

A 5-fold cross validation of daily GPP and ET was applied to test model-data mismatches as follows: each time data from four years were used for calibration and the remaining one-year data were used for validation. The model evaluation was based on combined validations of each year.

2.7. The difference between potential and actual productivity

The response of light-use efficiency to environmental factors such as light saturation, temperature, vapour pressure deficit and soil water status is non-linear. Thus, PRELES uses the environmental modifiers to describe how actual light use efficiency varies with each of a single environmental factor (Section A1). The potential photosynthetic production with given incident solar radiation during day k, the ϕ_k in Eq. (2), could be only partially achieved because of the suboptimal environmental and light interception conditions. All environmental modifiers $f_(i,k)$ are unitless and constrained between 0 and 1, while being calculated in parallel. Thus, the difference between potential daily photosynthetic productivity $P_(potential,\ k)$ (g C m^{-2} d^{-1}) and actual productivity P_k could be disaggregated and explained as a series of unachieved productivity $U_(i,\ k)$ (g C m^{-2} d^{-1}) due to unabsorbed light ($U_(APAR,\ k)$), light saturation limitation ($U_(L,k)$), temperature limitation ($U_(S,k)$), and water limitation ($U_(E,\ k)$):

$$P_{(potential,\ k)} - P_k = U_{(APAR,\ k)} + U_{(L,k)} + U_{(S,k)} + U_{(E,\ k)} \tag{7}$$

where

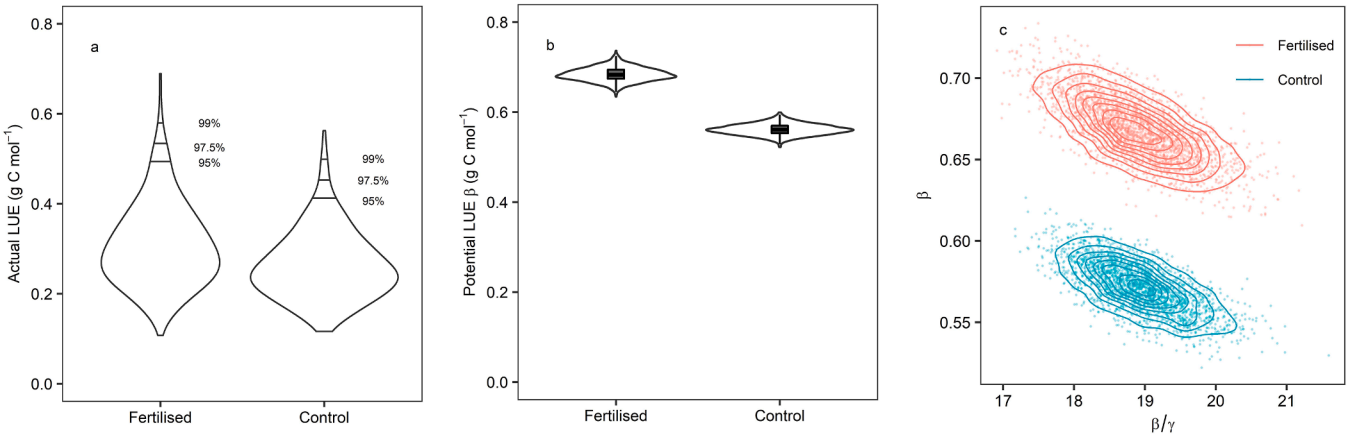

Fig. 1. Maximum or potential LUE (Light Use Efficiency) estimations. (a) The distribution of actual LUE and estimation of the maximum LUE defined as upper 95th, 97.5th and 99th percentiles based on eddy covariance derived observations of gross primary productivity and absorbed photosynthetic photon flux density. (b) Marginal posterior distribution of potential LUE parameter β. (c) Joint posterior distribution of maximum GPP (β/γ) and potential LUE β (Eq.2,3,4). This joint distribution was approximated by Markov Chain Monte Carlo simulation and shown as two-dimensional density.

$$P_{(potential,\ k)} = \beta \cdot \phi_k \tag{8}$$

$$P_k = \beta \cdot \phi_k \cdot f_{APAR,\ k} \cdot f_{L,k} \cdot f_{S,\ k} \cdot f_{E,k} \tag{9}$$

$$U_{APAR,\ k} = \phi_k \cdot \beta \cdot (1 - f_{APAR,\ k})$$

$$U_{L,k} = \frac{1 - f_{L,k}}{(1 - f_{L,k}) + (1 - f_{S,\ k}) + (1 - f_{E,k})} \cdot (1 - f_{L,k} \cdot f_{S,\ k} \cdot f_{E,k}) \cdot \phi_k \cdot \beta \cdot f_{APAR,\ k} \tag{10}$$

$$U_{S,k} = \frac{1 - f_{S,\ k}}{(1 - f_{L,k}) + (1 - f_{S,\ k}) + (1 - f_{E,k})} \cdot (1 - f_{L,k} \cdot f_{S,\ k} \cdot f_{E,k}) \cdot \phi_k \cdot \beta \cdot f_{APAR,\ k} \tag{11}$$

$$U_{E,\ k} = \frac{1 - f_{E,k}}{(1 - f_{L,k}) + (1 - f_{S,\ k}) + (1 - f_{E,k})} \cdot (1 - f_{L,k} \cdot f_{S,\ k} \cdot f_{E,k}) \cdot \phi_k \cdot \beta \cdot f_{APAR,\ k} \tag{12}$$

Considering that the water stress $f_{E,k}$ is the minimum of VPD stress ($f_{D,k}$) and soil water stress ($f_{W,k}$), the unachieved productivity due to water stress $U_{E,\ k}$ is either $U_{W,\ k}$ (unachieved productivity due to soil water stress) or $U_{D,\ k}$ (unachieved productivity due to VPD stress) according to the choice of $f_{E,k}$. The LUE framework quantitatively explained the daily variation of productivity with the above four reasons. Moreover, the explanations of daily variation can also be aggregated into annual level.

3. Results

3.1. Maximum actual LUE vs. potential LUE

The fertilised site showed higher maximum actual LUE and potential LUE, when compared with the control site (Fig. 1). The upper 97.5th percentile of actual LUE in the fertilised site was 0.53 g C mol^{-1}, and in the control was 0.45 g C mol^{-1}. Fertilisation changed the distribution of actual LUE towards longer tails (Fig.1a). The upper 99th percentile at the fertilised site was 15% higher than that at the control. For 97.5th percentile, actual LUE at the fertilised site was 16% higher, and for 95th was 20% higher. The comparison of maximum actual LUE might be inconclusive using percentiles, since both maximum and distribution of actual LUE vary largely among years (Fig. A2). The potential LUE estimates were ~24% higher than maximum actual LUE. When only β is set as site-specific, the MAP (maximum a posteriori probability estimate) in the fertilised plot was 0.66 g C mol^{-1},and 0.56 g C mol^{-1} in the control plot (Fig. 1b). When setting both β and γ as site-specific, values of γ on the two sites were similar, while values of β were distinctive (Fig. 1c). Thus, the differences between the two sites were distributed over the whole range of daily PPFD, including both the saturated productivity and the initial slope in the light response curve.

3.2. Daily photosynthetic capacity and light saturation

The estimates of maximum actual LUE were lower than the potential LUE at both sites (Fig. 1a, 1b). The key reasons included that actual photosynthesis was frequently restricted by light saturation and VPD-related stomatal conductance (Fig. 2a). The actual daily photosynthesis saturated when the daily PPFD reached 25-30 mol m^{-2} d^{-1}. However, PRELES simulated higher saturation points for the potential photosynthesis productivity by assuming optimal conditions of temperature, VPD, and soil water. In reality, those environmental factors were strongly correlated to each other in a seasonal pattern, which cannot be separated in the analysis of actual measurements (points in Fig. 2a). Despite large variations in the light-response of EC-based estimates of photosynthetic productivity, the distinction between the two sites was significant based on the paired t-test (p-value < 0.001) at both daily (Fig. 2a) and hourly level (Fig. 2b).

3.3. Partitioning the causes of increased GPP following N addition

The PRELES model simulations suggest that the fertilised site had 24% higher GPP than the control site (Table 2). This extra ecosystem GPP can be approximately partitioned to 17% increase in potential LUE and 7% increase in light interception (Table 2). Nitrogen addition led to higher LAI of both canopy and ground vegetation. The LAI of ground vegetation on the fertilised site was as much as twice that on the control site (Table 1). Because most light was already intercepted by the canopy, the fertilisation only increased the light interception by 7% (Fig. 3). This extra light interception was half due to canopy increase, and half due to the increase of ground vegetation. The higher productivity also led to higher evapotranspiration. The annual total evapotranspiration on the fertilised site was 19% (EC-based estimates) or 21% (PRELES-based estimates) higher than that on the control site (Table 2).

3.4. Environmental drivers of intra- and inter-annual GPP variation

In this high-latitude region, the seasonal pattern of potential GPP was based on the seasonality of temperature and incident solar radiation. Temperature limitation is crucial to explain the difference between potential and actual productivity from February to May (Fig. 4 & A5).

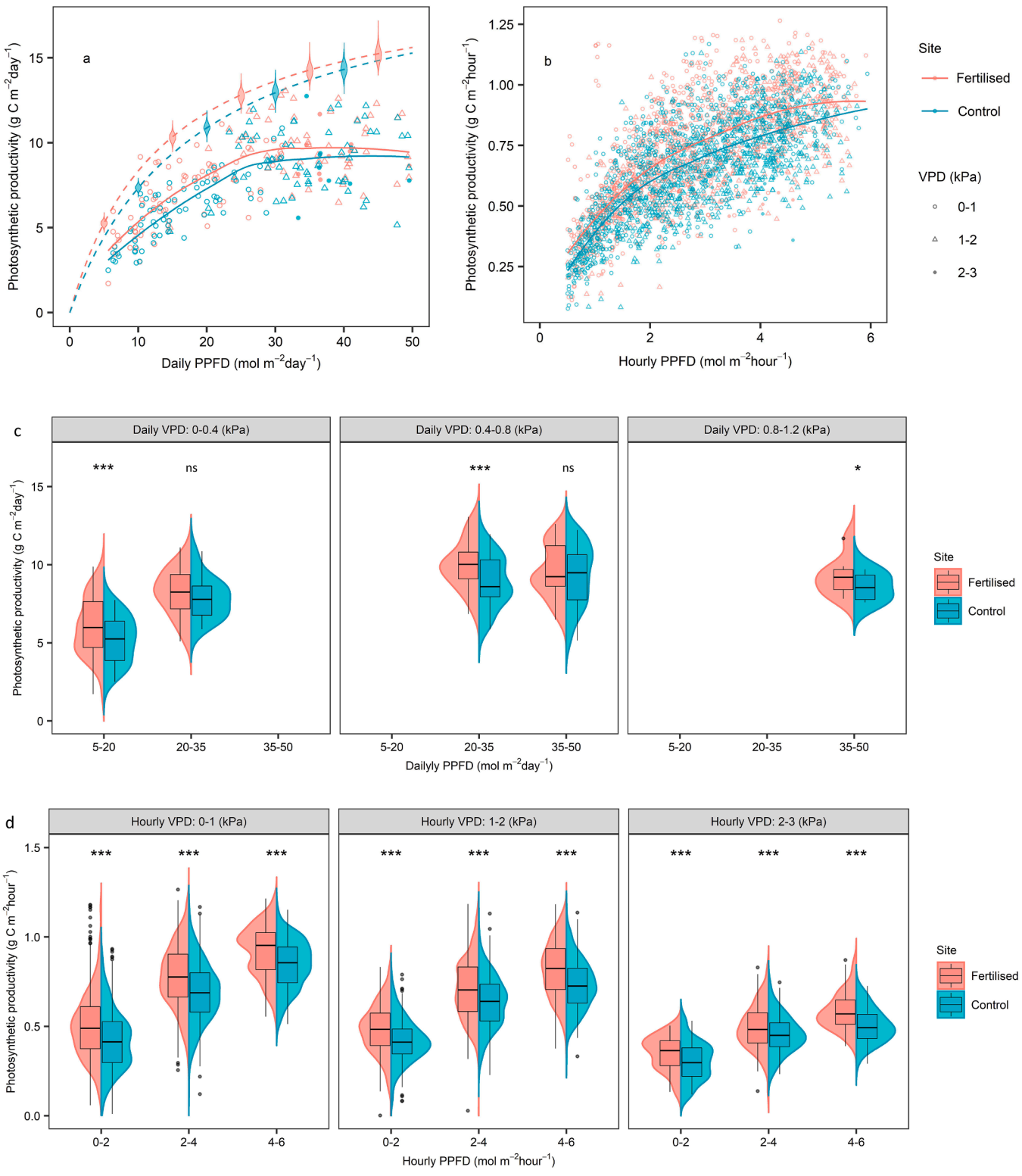

Fig. 2. Photosynthetic productivity on (a, c) daily and (b, d) hourly scales. The dashed lines in (a) show simulated light-saturated daily GPP estimated by PRELES (equation: $P = \beta \cdot Ø/(1 + \gamma \cdot Ø)$) using MAP (maximum a posteriori) parameters, assuming no limitations from temperature, VPD, or soil water. Violin plots in (a) present the parametric uncertainty. The points are the actual (a) daily GPP and (b) hourly GPP derived from eddy covariance measurements divided by f_{APAR}. Solid lines present the average based on LOESS smoothing. To avoid circular analysis, only records with QC (percentage of measured half-hourly data used to calculate daily value) larger than 0.7 was used in (a), and only measured data was used in (b). The points were divided into different PPFD and VPD classes (c, d). Significance of the difference between fertilised and control site for each class is determined by the paired t-test (ns = no significance, * p-value <0.05, ** p-value <0.01, *** p-value <0.001).

Table 2
Photosynthetic productivity from PRELES simulations (2014-2018) and eddy covariance (EC) data (2015-2018). Note: Annual GPP or ET was unavailable for 2014 because measurement started in August 2014.

	Fertilised site	Control site	Fertilised/ Control
Canopy f_{APAR} (August)	0.79	0.76	1.04
Understorey f_{APAR} (August)	0.08	0.05	1.6
Total f_{APAR} (August)	0.87	0.81	1.07
Potential LUE from PRELES (g C mol^{-1})	0.66	0.56	1.17
GPP of Trees from PRELES (MgC ha^{-1} yr^{-1})	10.29	8.52	1.21
GPP of ground vegetation from PRELES (MgC ha^{-1} yr^{-1})	1.03	0.62	1.66
Ecosystem GPP from PRELES (Mg C ha^{-1} yr^{-1})	11.32	9.14	1.24
Ecosystem ET from PRELES ($mmyr^{-1}$)	276	230	1.19
Ecosystem GPP from EC (Mg C ha^{-1} yr^{-1})	11.07	9.42	1.18
Ecosystem ET from EC ($mmyr^{-1}$)	296	243	1.21

The limitations from light saturation and VPD stress increased during May to August (Fig. A1 & A4) with higher intensity of radiation (Fig. 4). The limitation due to light saturation essentially disappeared as the days became shorter in September (Fig. 4).

Both soil water stress and VPD stress could lead to stomatal closure. The soil water stress played a negligible role at both sites, while VPD stress was a crucial component to explain the difference between potential and actual productivity during summer.

Actual annual GPP can be expressed as the difference between potential GPP ($P_{potential}$) and reductions in GPP (U_i) due to various limitations:

$$P = P_{potential} - U_{APAR} - U_L - U_S - U_E \quad (13)$$

Without considering the annual change of f_{APAR}, the variation of simulated annual GPP (g C m^{-2} yr^{-1}) between 2017 and 2018 on the control site can be portioned into: (1) changes in potential productivity due to the annual change of incident solar radiation ($\Delta P_{potential}$), (2) changes of unachieved GPP due to light saturation ΔU_L, (3) changes in temperature limitation ΔU_S, (4) changes in VPD stress ΔU_D , and (5) changes in soil water stress ΔU_W :

$$GPP_{2018} = GPP_{2017} + \Delta P_{potential} - \Delta U_L - \Delta U_S - \Delta U_D - \Delta U_W \quad (14)$$

$$871 = 810 + 384 - 184 + 91 - 202 - 27 \quad (15)$$

Increased intensity of solar radiation lifted both the potential productivity and the limitation in light saturation. Although photosynthesis started earlier in 2017 according to both model simulations and EC measurements (Fig. 6), the acclimation process was faster in 2018 due to the rapid increase in temperature in May 2018. The main water stress for stomatal closure switched from VPD to soil water for only one week on the control site because of a drought event in 2018 (Fig. 4b). Otherwise, the main source of water stress was via increased VPD. In comparison with the control site, the plants at the fertilised site seemed to be more sensitive to the increasing VPD (Fig. A3). The optimum day temperature of plants at the fertilised site was higher than that at the control (Fig. A5, Eq. (A3), Eq. (A4), Eq. (A5), Table A2).

3.5. Cross validation and uncertainty quantification

PRELES effectively explained the daily variation of both GPP and ET, and covered the randomness of data by the predictive uncertainty (Fig. 6, Fig. A7). Because of measurement uncertainty of the EC method, the observations of the two sites could be distinctive even on the same day with the same environmental conditions. The LUE differences between the two sites can be detected from EC data, but require strict data filtering to avoid large biases. PRELES was applied to detect the noise (the grey area in Fig. 6, Fig. A7). The model calibration is a compromise between the two sites since most of the parameters were shared, which lessened the chance of overfitting. The lower the data quality was, the larger was the bias of GPP, especially when QC was less than 0.2 (Fig. A8).

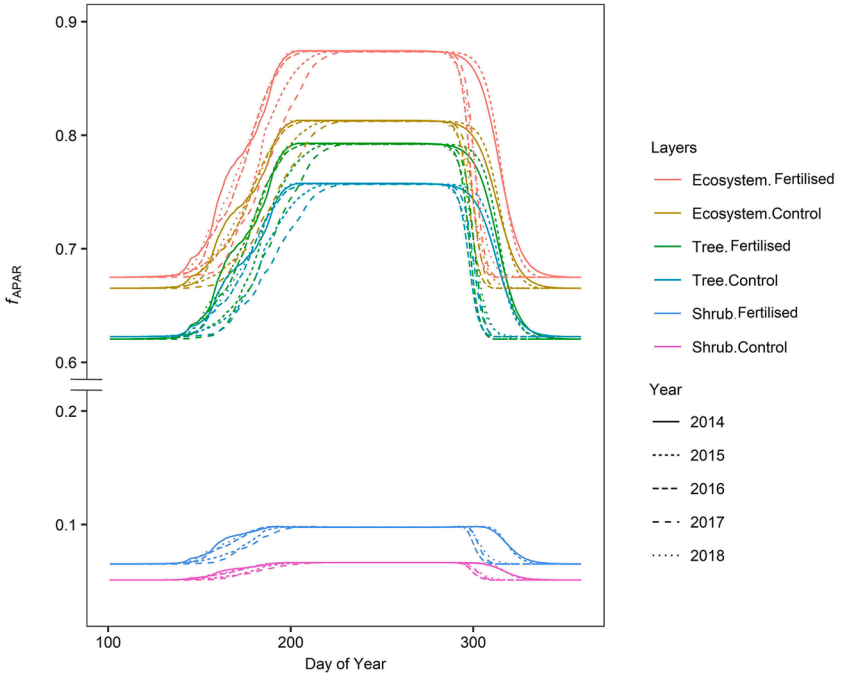

Fig. 3. Seasonal variation in fraction of absorbed PPFD (f_{APAR}).

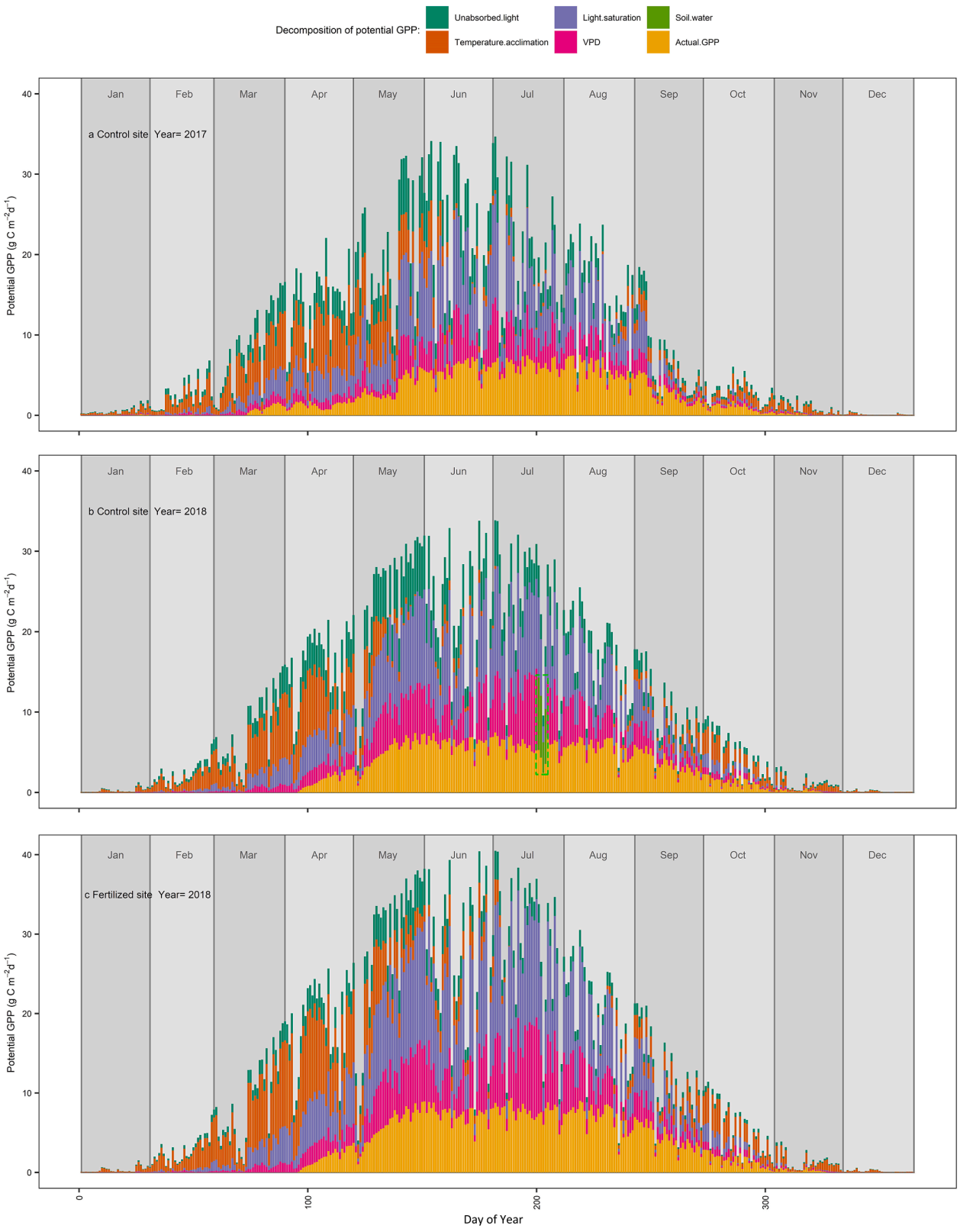

Fig. 4. Disaggregated potential gross primary production (GPP) based on PRELES simulations for the control site in (a) 2017 and (b) 2018, and (c) the fertilised site in 2018. The reduction of GPP due to soil water stress was marked with a bright green dashed rectangle (b).

4. Discussion

4.1. Daily light saturated GPP

Following nitrogen fertilisation, boreal conifers expand the photosynthetic apparatus by increasing the nitrogen concentration within foliage (Linder and Troeng, 1980; Tamm, 1991). Leaf nitrogen concentration has been shown to correlate with the light-saturated rate of photosynthesis (P_{max} in Eq. (4) or β/γ in Eq. (2), (3)) at leaf or shoot level (Field and Mooney, 1986; Evans, 1989; Reich et al., 1995, 1997; Wright et al. 2004). Peltoniemi et al. (2012a) reported that potential LUE, i.e. the slope of GPP vs. PPFD under low PPFD (q in Eq. (4) or β in Eq. (2)), correlated significantly with foliage mean nitrogen concentrations at canopy level, although the relation became insignificant when considering the correlation between β and γ. Our controlled experiment avoided the disturbances from variations in climate and tree species, and illustrated a distinctively higher potential LUE in the fertilised plot even when considering the parameter correlation (Fig. 1c). Both potential and actual LUE showed a difference between the sites even under low PPFD (Fig. 2). Irrigation and fertilisation experiments (Ewers et al. 2000; Ewers et al., 2001) have demonstrated that fertilisation decreased mean canopy stomatal conductance in the absence of irrigation, as a result of the production of fine roots with low saturated hydraulic conductivity. Since higher daily PPFD correlated with higher VPD, the difference of actual photosynthetic productivity between fertilised and control sites decreased under high PPFD (Fig. 2) most likely due to the reduced stomatal conductance of the canopy.

Our conclusions differ from those of a previous study in the same stands by Tarvainen et al. (2016) who did not detect a difference in daily shoot photosynthesis and actual LUE between the stands, even though leaf nitrogen concertation was higher in the fertilised stand (Table A3). Tarvainen et al. (2016) studied shoot-level actual LUE, defined as shoot photosynthesis divided by incoming PPFD, and estimated the mean daily LUE for August 2013 by scaling up shoot chamber measurements at different locations in the canopy. Their shoot-level actual LUE declined with increasing PPFD in much the same way as $\beta/(1+\gamma\varnothing)$ in the present study, with similar values for low PPFD, which approximates the potential LUE in both studies (Fig. 7). The decline of shoot-level actual LUE with increasing PPFD in Tarvainen et al. (2016) is somewhat faster than that of $\beta/(1+\gamma\varnothing)$ in this study, probably because of correlations between PPFD and other limiting factors, notably VPD. We note that the differences between the two stands detected in field measurements are small in comparison with the possible uncertainties involved in the scaling up of instantaneous shoot level measurements to daily or seasonal canopy-level values. We furthermore need to bear in mind that the present study includes the contribution of the understorey to the ecosystem LUE, assuming the same photosynthesis parameters for both canopy layers. It is possible that the observed increase in LUE is mostly attributable to the understorey, for example, through a change of the understorey community structure towards photosynthetically more efficient species. This remains to be explored in future studies.

4.2. Contribution of understorey to ecosystem GPP

Palmroth et al. (2014) found that increased overstorey shading and constrained water supply overrode the positive effects of nitrogen addition on photosynthesis of understorey shrubs in boreal *Picea abies* and *Pinus sylvestris* stands. In our experiment, these abiotic factors exist only as weak impacts on ecosystem productivity. The degree of canopy closure allocates solar energy between trees and understorey plants. The light availability for the understorey was slightly reduced in the fertilised plot compared to the control plot based on the calculation from Eq. (1). However, the nitrogen addition plots showed considerably larger biomass of ground vegetation with higher LAI (Table 1) and greater cover of bilberry (*Vaccinium myrtillus* L.), all of which entirely compensated the effects of increased shading from the tree canopy. One reason could be that trees outcompete understorey in competition for soil resources on the control site, while the ground vegetation on the fertilised site intercepts and sequesters nitrogen before uptake by tree root systems when the treatments were performed on soil surface (Nordin et al., 1998; Bobbink et al., 2010). With increased LUE and light interception, the fertilised plot showed 66% higher GPP in the understorey and 21% higher GPP in the canopy, in comparison to the control site. The phenology of the forest floor vegetation as a whole has been reported to be similar to the phenology of Scots pine (Kolari et al., 2006). Even though there are differences in the photosynthesis physiology between understorey and overstorey vegetation (Palmroth et al., 2014; Lim et al., 2015) with the lack of quantitative information, we assumed that overstorey and understorey share the same potential LUE and respond similarly to changing environment. Therefore, the difference of understorey contribution to ecosystem GPP between the fertilised and the control plot is assumed to arise from differences in their light interception. With these assumptions, the understorey (shrubs) contributed 9% of ecosystem GPP in the fertilised site and 7% in the control site. Furthermore, sunflecks that expose leaves in shade plants in

Table A1
Climate summary.

Year	2014	2015	2016	2017	2018
Mean air temperature (°C)	4.0	3.9	3.0	2.1	2.1
Effective temperature sum (+5°C)	1189	999	1086	828	1219
Precipitation (mm)	692	553	521	593	448
Potential evapotranspiration (mm)	670	665	661	604	662
Actual evapotranspiration of fertilised site from EC data (mm)	-	339	339	229	284
Actual evapotranspiration of control site from EC data (mm)	-	254	282	199	233
UNEP aridity	1.03	0.83	0.79	0.98	0.68

Note: Potential evapotranspiration was calculated using both Makkink and Thornthwaite equations (Thornthwaite, 1948; De Bruin, 1981; McMahon et al., 2012), and the averages from the two methods are shown here. UNEP (United Nations Environment Programme) aridity (Middleton and Thomas, 1992) is the ratio between precipitation and potential evapotranspiration. The climate is often considered as humid when UNEP is larger than 0.65.

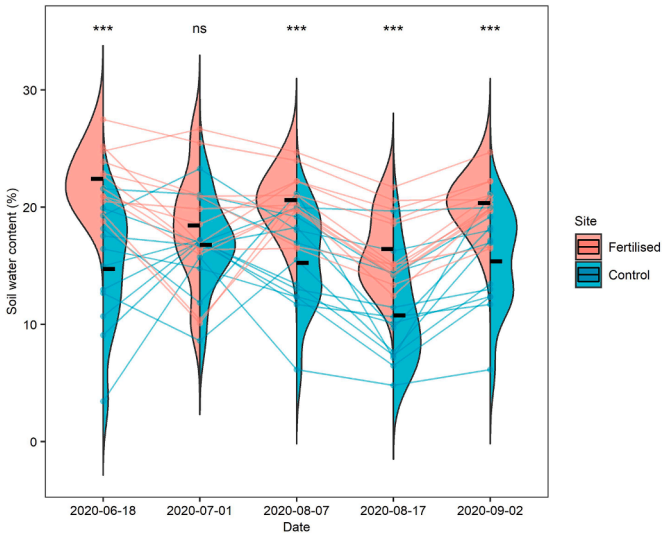

Fig. 5. Spatial heterogeneity of soil moisture in the upper 0-6 cm layer and the comparison between fertilised and control sites. The violin plot represents the probability density of the soil moisture data for each plot on the given day. The black horizontal bar marks the average of the plot, and each connected line represent measurements from one fixed position within the site. Significance of the difference between fertilised and control site for each day was determined by the paired t-test (ns = no significance, * p-value <0.05, ** p-value <0.01, *** p-value <0.001).

Table A2
Parameters in PRELES, soil moisture measurement error module and likelihood function.Note: The parameters PRELES are ordered by their sensitivity to the model outputs (Peltoniemi et al., 2015). MAP = maximum a posteriori parameter vector, GPP = gross primary production, ET = evapotranspiration, SWC = soil water content.

Symbol	Equation	Meaning	Units	Prior minimum	Prior maximum	MAP in site-specificcalibration		MAP in multisite calibration	
						Fertilised	Control	Fertilised	Control
χ	(A10)	Evaporation parameter	$dm^3\ mol^{-1}$	0	2.5	0.0539	0.0664	0.0572	
γ	(3)	Light modifier parameter for saturation with irradiance	$mol^{-1}\ m^{-2}$	1e-4	0.5	0.0315	0.0303	0.0311	
α	(A10)	Transpiration parameter	mm $(g\ C\ m^{-2} kPa^{1-\lambda})^{-1}$	1e-6	10	0.309	0.285	0.293	
X_0	(A4)	Threshold for state of acclimation change	°C	-10	10	-5.06	-4.74	-5.01	
β	(2)	Potential light-use efficiency	$g\ C\ mol^{-1}$	0.2	2.5	0.617	0.591	0.662	0.564
S_{max}	(A3)	Threshold above which the acclimation modifier reaches its maximum	°C	5	25	19.8	17.6	19.2	
λ	(A10)	Parameter adjusting water-use efficiency with vapour-pressure deficit	-	1e-4	0.999	0.760	0.703	0.732	
ρ_P	(A8)	Threshold for the effect of soil-water stress on photosynthesis	-	0	0.999	0.711	0.366	0.582	
ν	(A10)	Parameter adjusting water-use efficiency whether soil water limits gross primary production	-	1e-4	2.5	0.765	0.857	0.801	
κ	(A7)	Sensitivity parameter for vapour-pressure deficit response	kPa^{-1}	-1	-1e-3	-0.193	-0.171	-0.191	
ρ_E	(A11)	Threshold for the effect of soil-water stress on evaporation	-	0	0.999	0.655	0.725	0.748	
τ	(A5)	Delay parameter for ambient temperature response	-	1	25	6.75	5.53	5.99	
θ_{FC}	(A9)	Effective field capacity	%	-	-	29.8	20.2	25.6	16.8
τ_F	(A13)	Delay parameter of drainage	-	1	5	2.87	1.21	3.02	1.57
r	(6)	Weight of soil measurement at 15cm depth for estimating the average soil water content	-	0	1	0.826	0.945	0.786	0.964
s	(6)	Bias in the representative of the soil moisture measurement sensor	-	0.5	1.5	1.21	1.35	1.27	1.30
a_{GPP}	(5)	Random measurement uncertainty parameter of GPP	$g\ C\ m^{-2}$	1e-4	5	0.237	0.211	0.332	0.247
b_{GPP}	(5)	Random measurement uncertainty increases with the magnitude of daily GPP measurement	-	1e-4	3	0.0845	0.0948	0.0745	
a_{ET}	(5)	Random measurement uncertainty parameter of ET	mm	1e-4	5	0.0688	0.0433	0.0652	0.0558
b_{ET}	(5)	Random measurement uncertainty increases with the magnitude of daily ET measurement	-	1e-4	3	0.146	0.179	0.148	
a_{SWC}	(5)	Random measurement uncertainty parameter of SWC	%	1e-4	50	2.33	7.38	3.49	6.28
b_{SWC}	(5)	Random measurement uncertainty increases with the magnitude of daily SWC measurement	-	1e-4	3	0.285	0.164	0.172	

the understorey to short periods of bright light might also introduce large noise into the calculations (Chazdon and Pearcy, 1991).

4.3. Assessment of the drought impact on GPP

The drought of 2018 in the Nordic region was considered as severe with a long-lasting and large soil water deficit (Lindroth et al., 2020). The absence of precipitation in May and July of 2018 (Fig. A1) coincided with warmer temperature and lower relative humidity, resulting in higher atmospheric water demand (Table A1) and lower soil water content (Fig. A3). Fertilisation has been reported to increase both aboveground litter production and fine root turnover (Leppälammi-Kujansuu et al., 2014). The soil organic matter layer was thicker at the fertilised site, possibly leading to the observed difference in field capacity between the sites (Table 1 & A2, Fig. 5 & A3). Although the evapotranspiration of the fertilised site was much higher than that of the control site, the soil of the control site was drying faster after rain events (Fig. 5 & A3, drainage parameter in Eq. (A13), Table A2). The soil water content was distinctively different between the two sites, especially in the top layer. The faster biomass growth and turnover due to fertilisation may have changed the soil properties, which may have affected the soil water balance.

Distinguishing the daily effects of soil moisture supply and atmospheric water demand is difficult due to their strong correlation and the lack of tools for manipulating atmospheric demand in field experiments (Novick et al., 2016). Here the PRELES simulations were designed to isolate the impact from VPD stress and soil water stress. Although the precipitation in 2018 largely decreased, the effect of soil water limitation was still negligible (Eq. (15), Fig 4, Fig. A6). Instead, high atmospheric water demand became more critical in constraining GPP during the warmer and drier year. Global climate datasets have revealed a sharp increase of VPD after the late 1990s (Simmons et al., 2010; Willett et al., 2014). Correspondingly, earth system models have consistently projected continuous increases of VPD throughout the current century (Yuan et al., 2019). Along with the global warming, the relative importance of atmospheric water demand will keep increasing as higher temperatures may result in elevated VPD.

4.4. Discrepancies between PRELES simulations and EC measurements

It is common to have gaps in high temporal resolution (e.g., half-hourly) EC data which requires gap-filling by either interpolation or look-up tables derived from measurements under similar situations in terms of vegetation status and meteorological conditions (Aubinet et al., 2012). Various factors, such as site conditions and gap length, affect the reliability of these gap-filled data (Moffat et al., 2007). Minunno et al. (2016) found that different quality control selection strategies of the training EC data led to similar parameter estimates and predictions of PRELES for most boreal coniferous forests. Thus, in return, the robustness of PRELES predictions provides a reliable reference for validating aggregated EC data. For instance, the daily GPP observations in EC data were detected as biased when QC was less than 0.2 (Fig. A8a) for our sites.

Table A3
Leaf nitrogen per unit leaf mass (N_m) for fertilised (F) and control (C) treatments. Note: Data of *Vaccinium myrtillus* is from *Picea abies* standsat Svartberget. Data of *Vaccinium vitis-idaea* is from*Pinus sylvestris* stands at Åheden. These two experiments are about 6 to 7 km apart from the experimental forest presented in our study (Rosinedalsheden). The nitrogen additions for all the fertilised sites was the same, 50 kg N ha^{-1} $year^{-1}$, except that samples of Ericaceous leaves were collected in Rosinedalsheden from 2010 to 2011when the nitrogen additions were 100 kg N ha^{-1} $year^{-1}$ (section 2.1).

Species	Leaf positionin canopy	Leaf age (yr)	N_m (mg g^{-1})		Reference
			F	C	
Pinus sylvestris (Rosinedalsheden)	Upper	0	18.8 (1.6)	11.3 (1.0)	Tarvainen et al. (2016)
		1	24.2 (1.7)	12.0 (2.1)	
		2	25.8 (3.2)	10.5 (1.9)	
	Mid	0	16.8 (1.5)	11.4 (0.7)	
		1	23.2 (0.9)	12.7 (0.8)	
	Loweriom	0	17.8 (3.1)	12.0 (1.2)	
		1	22.9 (2.2)	13.0 (0.9)	
Ericaceousdwarf shrubs (Rosinedalsheden)		-	16.2 (4.0)	11.6 (1.0)	Hasselquist et al. (2016)
Vaccinium myrtillus (Svartberget)		0	22.3 (0.9)	16.2 (0.8)	Palmroth et al. (2014)
Vaccinium vitis-idaea (Åheden)		0	13.2 (0.7)	10.4 (0.4)	
		1	10.8 (0.7)	8.8 (0.1)	

4.5. Temporal and spatial variation of nitrogen supply

Satellite-driven LUE models have been widely used for monitoring geographical variation of ecosystem productivity (e.g. Potter et al., 1993; Sims et al., 2008; Yuan et al., 2007; Zheng et al., 2018). However, they commonly assume higher frequency variation to occur only in PPFD, temperature, and VPD, whereas nitrogen supply to remain constant. Although with much less nitrogen addition than this fertilisation experiment, nitrogen deposition has been globally observed, altering the nitrogen status of forest ecosystems (Bedison and McNeil, 2009; Dezi et al. 2010; Fang et al. 2011; Fleischer et al. 2013). Benefited from continuous development of remote sensing techniques for efficiently quantifying foliar nitrogen concentration and nitrogen spatial variability (e.g. Thomas and Oerther, 1972; Martin and Aber, 1997; Martin et al., 2008; Wang et al., 2016; Loozen et al., 2020), accurately integrating the impacts of changing nitrogen status on regional or global vegetation production is or may soon be feasible. Currently, the reliability of remote sensing estimates of foliar nitrogen content varies with species, sites, and methods (Watt et al., 2019). Furthermore, the accuracy evaluation has been mainly aimed at the nitrogen difference between species and ecosystems (e.g. Ferwerda and Skidmore et al., 2007; Martin et al., 2008; Wang et al., 2016), rather than within individual species (e.g. Stein et al., 2014). This study disaggregated the effects of nitrogen addition on GPP, which might provide a reference for LUE models to map and forecast forest production in response to temporal and spatial variation of nitrogen supply on large geographical scales.

5. Conclusion

Nitrogen fertilisation considerably elevated both ecosystem light interception (i.e. increase in canopy LAI) and LUE. Using an ecosystem flux model calibrated with empirical data we were able to show that most of the improved productivity could be explained by the higher potential LUE.Although the increased canopy cover resulted in lower light availability for ground vegetation in the fertilised plot, this was compensated by higher foliage biomass and LUE resulting in greater productivity of the understorey due to fertilisation. The stand-level LUE divergence between fertilised and control sites occurred on both low and high daily PPFD conditions. The constraint from atmospheric water demand, instead of soil water stress, dominated the variation of ecosystem GPP during drought events. The controlled field experiment provides the necessary data for the construction and refining of hypotheses concerning the nitrogen addition effect. Meanwhile, the inverse modelling approach provides a particularly powerful tool for the quantitative description and disaggregation of measured variation of ecosystem GPP.

Declaration of Competing Interest

The authors declare that they have no known competing financial interests or personal relationships that could have appeared to influence the work reported in this paper.

Acknowledgements

We acknowledge the contributions of Knut and Alice Wallenberg Foundation (#2015.0047), the Horizon 2020 Research and innovation framework program (Forest Carbon Flux and Storage Mapping Service, proposal #821860), the Swedish Infrastructure for Ecosystem Science (SITES), and the Strategic Research Council at the Academy of Finland (IBC-CARBON, decision. #312635, SOMPA 312912).

Appendix

Section A1 Environmental modifiers of PRELES

Daily photosynthetic production during day k, P_k, is predicted as follows:

$$P_k = \beta \cdot \phi_k \cdot f_{APAR,\,k} \cdot \prod_i f_{i,k} \tag{A1}$$

where β is the potential LUE (g C mol^{-1}), ϕ_k the PPFD (mol m^{-2} d^{-1}) and $f_{APAR,\,k}$ the fraction of ϕ_k absorbed by the canopy during day k. An array of modifiers $f_{i,k}$, varying between 0 and 1, accounts for the impacts of environmental conditions.

The saturation of photosynthetic production with high PPFD during day k is expressed by the light modifier $f_{L,k}$, that follows the rectangular-hyperbola photosynthesis model (Mäkelä et al., 2008):

$$f_{L,k} = \frac{1}{\gamma \varnothing_k + 1} \tag{A2}$$

where γ (m^2 mol^{-1}) is an empirical parameter.

Temperature impacts photosynthesis using a modifier that accounts for temperature acclimation ($f_{S,k}$) (Mäkelä et al., 2004; Mäkelä et al., 2008):

$$f_{S,k} = \min(S_k / S_{max}, 1) \tag{A3}$$

$$S_k = max(X_k - X_0, 0) \tag{A4}$$

$$X_k = X_{k-1} + \frac{1}{\tau}(T_k - X_{k-1}) \tag{A5}$$

where T_k (°C) is daily air temperature of day k. X_k is calculated using a first-order dynamic delay model influenced by the temperature T_k and the value of X_{k-1} during the previous days (X_{k-1}). The parameter τ, expressed in days, represents the speed of response of the current acclimation status to changes in temperature. S_k (°C) is the state of acclimation that depends on the lower temperature limit parameter X_0 (°C) above which f_S is higher than 0 and on the state of acclimation. S_{max} (°C) is the minimum temperature threshold parameter at which canopy photosynthesis is not limited by low temperatures (i.e., $f_{S,k}$= 1 for $S_k \geq S_{max}$).

Plant water stress ($f_{E,k}$) reduces photosynthesis and it can be caused by vapour pressure deficit of the atmosphere ($f_{D,k}$) and soil water availability ($f_{WP,k}$). We assumed that for a given day k only the most limiting factor between $f_{D,k}$ and $f_{WP,k}$ reduces photosynthesis (Landsberg and Waring, 1997).

$$f_{E,k} = \min\left(f_{D,k}, f_{WP,k}\right) \tag{A6}$$

The $f_{D,k}$ affects GPP through an exponential relationship:

$$f_{D,k} = e^{\kappa D_k} \tag{A7}$$

where D_k (kPa)average VPD during day k and κ (kPa^{-1}) is an empirical parameter assuming typically negative values.

The soil water modifier $f_{WP,k}$ depends on the relative extractable water W_k

$$f_{WP,k} = \min(1,\ W_k / \rho_P) \tag{A8}$$

$$W_k = \frac{\theta_{soil,k} - \theta_{WP}}{\theta_{FC} - \theta_{WP}} \tag{A9}$$

where $\theta_{soil,k}$ is water stored in the soil, $\theta_{WP}$is the wilting point and θ_{FC} is the field capacity, and ρ_P is the threshold parameter of W_k (relative extractable water) below which P_k is reduced linearly.

Section A2 Evapotranspiration and soil water module of PRELES

The daily ET during day k, E_k, is simulated as follows:

$$E_k = \alpha \cdot P_k \cdot f_{WP,k}^{v} \cdot D_k^{1-\lambda} + \chi \cdot \left(1 - f_{APAR,k}\right) \cdot \phi_k \cdot f_{WE,k} \cdot \frac{s_{DS,k}}{s_{DS,k} + p_{psychrom}} \tag{A10}$$

$$f_{WE,k} = \min(1,\ W_k / \rho_E) \tag{A11}$$

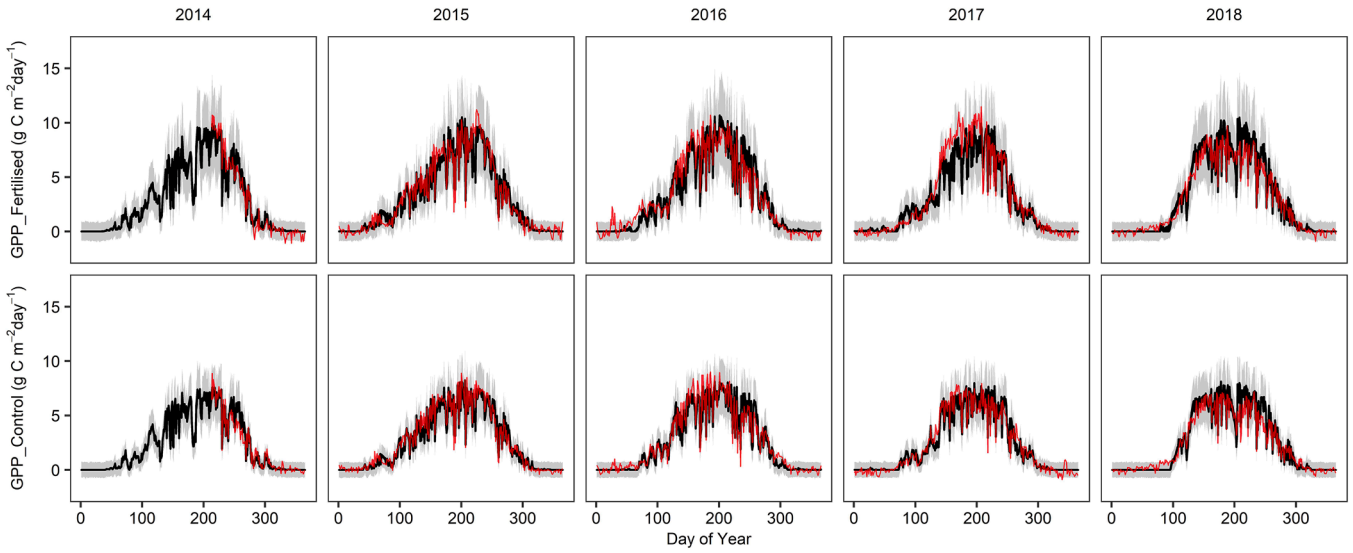

Fig. 6. Daily gross primary production. The red lines are eddy covariance observations without being filtered by the quality control flag. Black area is parametric uncertainty (negligible). Grey area is the predictive uncertainty that describes the possible ranges of the mismatches between PRELES and eddy covariance measurements. The uncertainty was quantified as 95% Bayesian credible intervals.

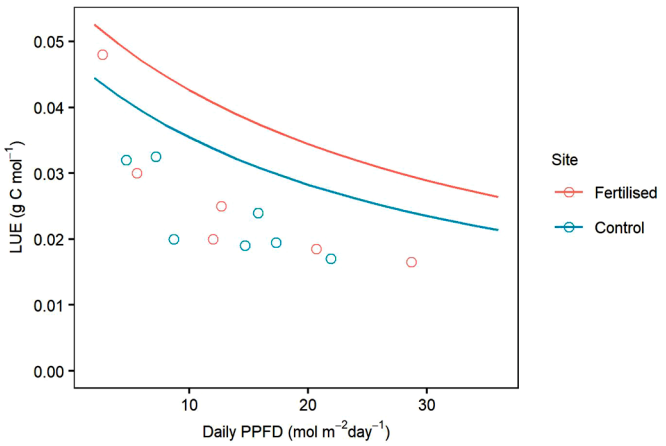

Fig. 7. Comparison of actual shoot-level daily LUE (Tarvainen et al. 2016) (circles) and $\beta/(1+\gamma\varnothing)$ (lines) as functions of PPFD ($\varnothing$). The MAP (maximum a posteriori) values for control and fertilised stand from the calibration for both β and γ (Fig. 1c) were used in the lines.

where α is a transpiration parameter, χ an evaporation parameter and λ an adjustment parameter for the effect of VPD on transpiration on day k. The $f_{WP,k}$ is raised to the power ν, since the response of E_k to soil-water stress may differ from that of P_k. For the evaporation part, $s_{DS,k}$ is the slope of the relationship between the saturation vapour pressure (kPa) and air temperature (°C), and $p_{psychrom}$ is the psychrometric constant (Campbell, 1977) that relates the partial pressure of water in air to the air temperature (kPa °C^{-1}). The modifier $f_{WE,k}$ accounts for the suboptimal condition of evaporation due to soil water, and ρ_E is the threshold parameter of W_k (relative extractable water) below which evaporation is reduced linearly.

Soil water storage θ_{soil} (mm) are described by a simple bucket module in PRELES:

$$\theta_{soil,k} = \theta_{soil,k-1} + R_k + M_k - F_k - E_k \tag{A12}$$

$$F_k = \frac{\theta_{soil,k-1} - \theta_{FC}}{\tau_F} \tag{A13}$$

where R_k (mm) is rainfall exceeding canopy water storage capacity on day k, M_k (mm) is snowmelt, F_k(mm) is drainage from the soil, and E_k (mm) is the evapotranspiration. When soil water storage accumulates up to the field capacity of soil (θ_{FC}), additional water drains away from the system with a fix time constant (τ_F). Precipitation is assumed to be snow when air temperature is below 0 °C. The dynamic of intercepted water on canopy surfaces and the water accumulated as snow/ice are calculated in parallel (Peltoniemi et al., 2015).

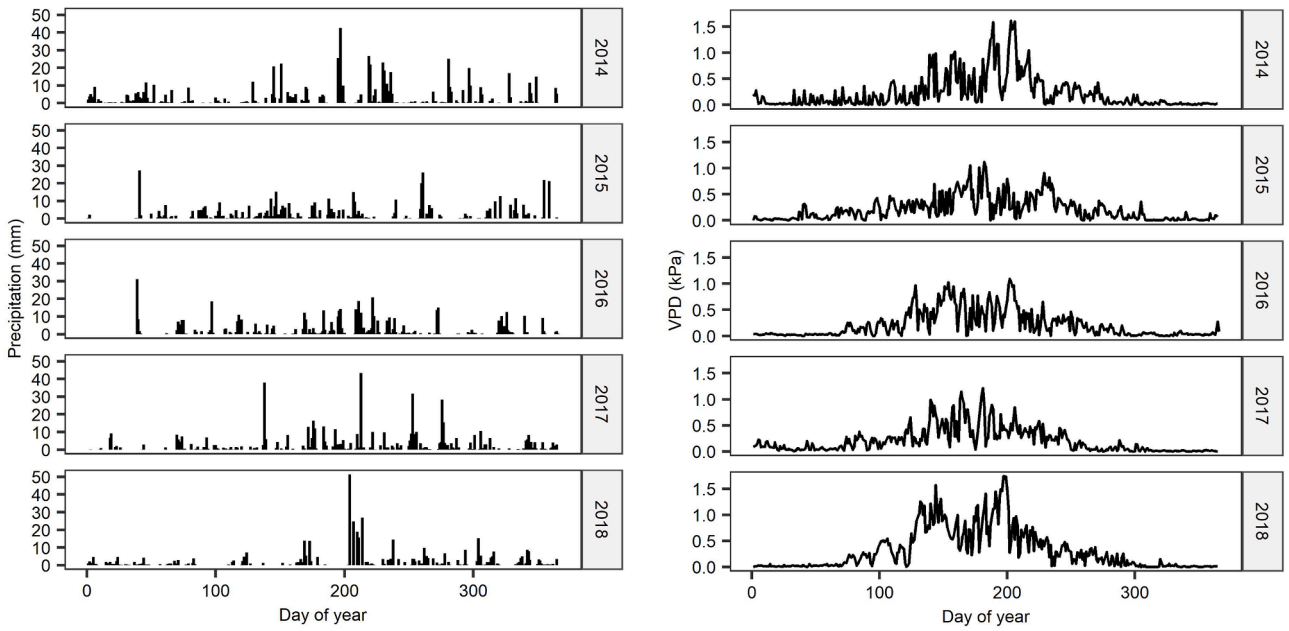

Fig. A1. Precipitation and VPD observations from 2014 to 2018.

Section A3 Measurement bias in soil moisture status

A quantitative explanation of forest productivity is commonly limited due to data collection and knowledge of physiological process, which causes problems associated with inference. Assessing the role of water stress associate even with more problems because of the random measurement uncertainty (Fig. A3) and within-site spatial heterogeneity (Fig. 5) in soil moisture status. The measurement error module (Eq. (6)) was designed for the soil moisture data and integrated into the PRELES calibration. This bias correction in the soil moisture sensor mainly relies on the balance between precipitation and evapotranspiration data. One concern that might occur about this bias correction is that the outcomes and presented results could be just an artefact of model derivation. Thus, we implemented a sensitivity analysis on the relation between soil moisture data and model calibration to show how the soil moisture measurement error affected our model calibration and predictions.

In this test, the bias correction module was dropped. We assume that fertilised and control sites shared the same water moisture data, the average of the two sensors. We also assumed the soil moisture measurement at 15 cm depth to be the average soil water content of the depth explored by plant roots. Bias was manually added to the soil moisture data from -50% to +50% to generate 11 sets of virtual soil moisture data. Then calibrations of PRELES were implemented for the 11 datasets respectively.

When compared with current GPP and ET estimations (Table 2, Fig. 6 & A7), the 11 virtual-data based calibrations performed a maximum 4% difference in the average of annual GPP prediction, and a maximum 12% difference in the average of annual ET (Fig. A9). Different biases also affected our inference about the severity of drought in 2018. The ratio between annual unachieved productivity due to soil water stress (U_W) and actual annual GPP in 2018 varied from 0% to 5% for the 11 virtual datasets. The ratio of annual unachieved productivity due to VPD stress (U_D) to actual GPP varies from 52% to 85%. Considering that PRELES can be calibrated even without using soil moisture data (Tian et al., 2020), the error propagated from soil moisture data to GPP predictions is negligible. However, our inference on the severity of drought might be affected or be introduced a certain amount of uncertainty.

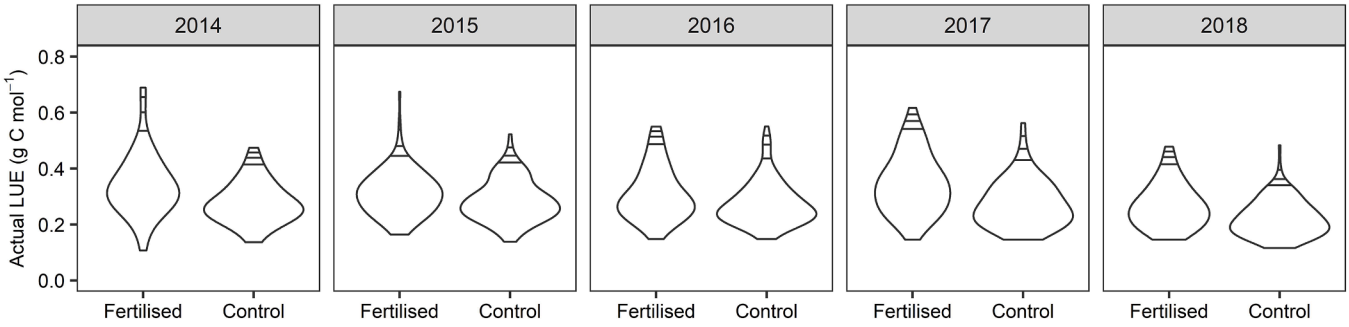

Fig. A2. The distribution of actual LUE and estimation of the maximums LUE defined as upper 95th, 97.5th, and 99th percentiles (the three horizontal lines marked in the each violin plot) of each year. LUE = light use efficiency.

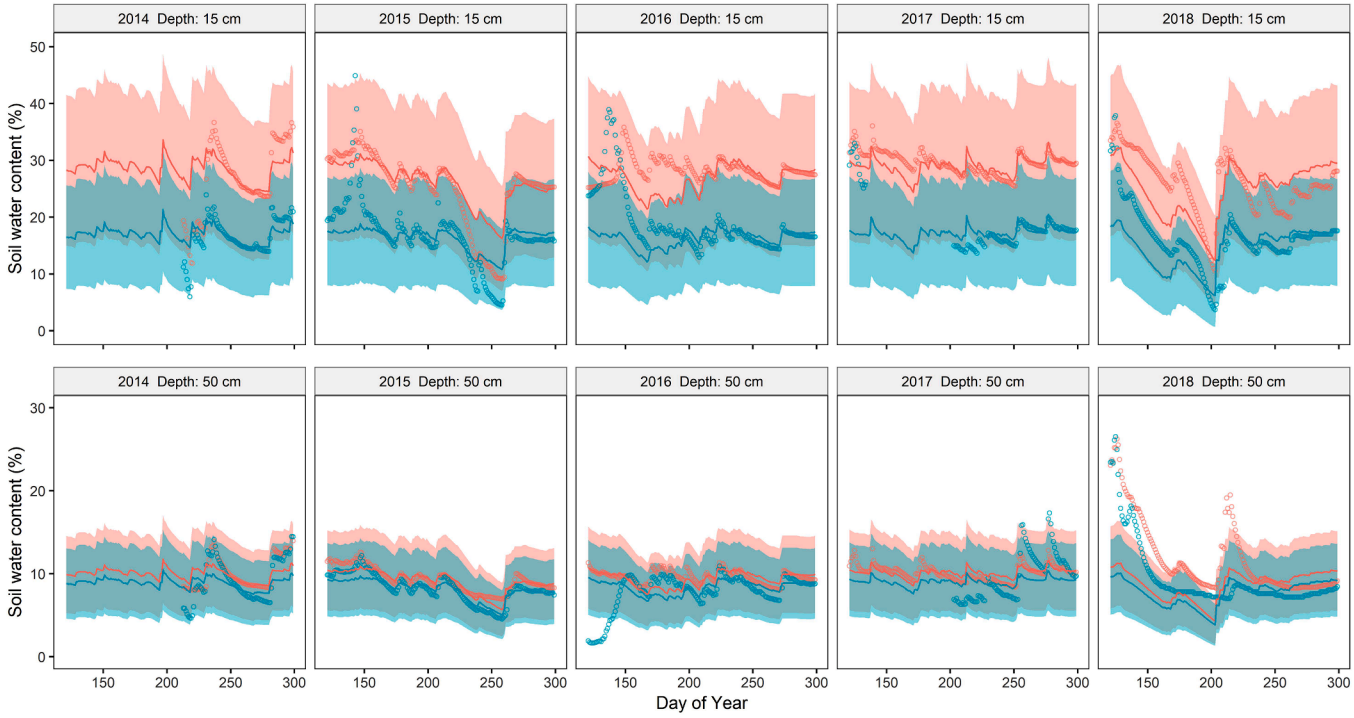

Fig. A3. Soil water content of the fertilised (red) and control (cyan) sites from measurements and model simulations in the depth of 15cm and 50cm. The circles are observations with biases corrected. Solid lines are simulations from PRLES. Light ribbons are 95% Bayesian credible intervals.

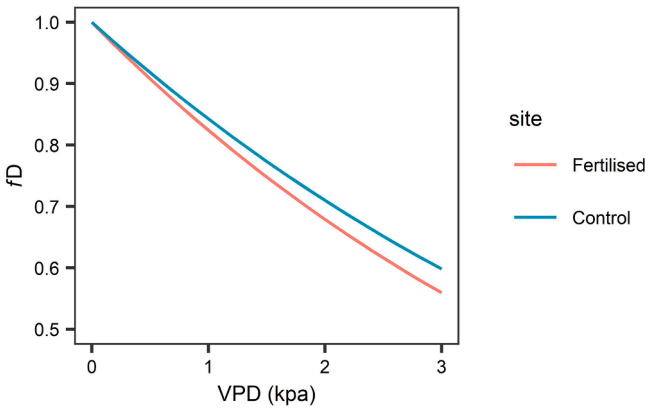

Fig. A4. Sensitivity of daily photosynthetic production to VPD (vapour pressure deficit). Modifiers f_D is constrained between zero and one, representing the impact of VPD on daily photosynthetic production.

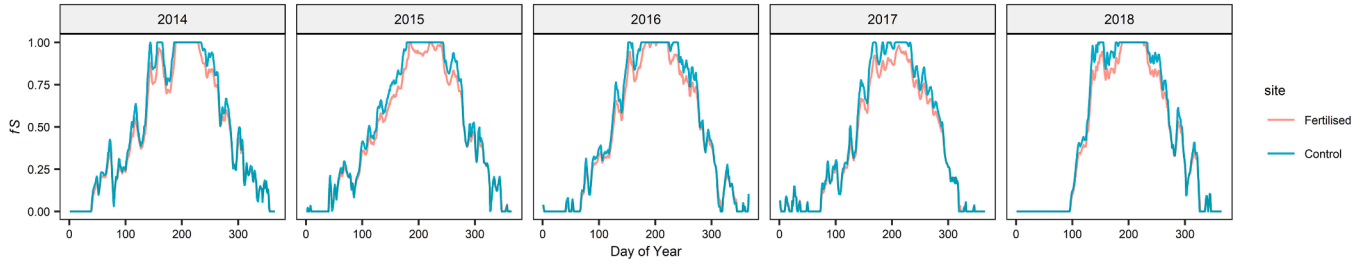

Fig. A5. Temperature acclimation processes. Modifiers f_S is constrained between zero and one, representing the impact of temperature on daily photosynthetic production.

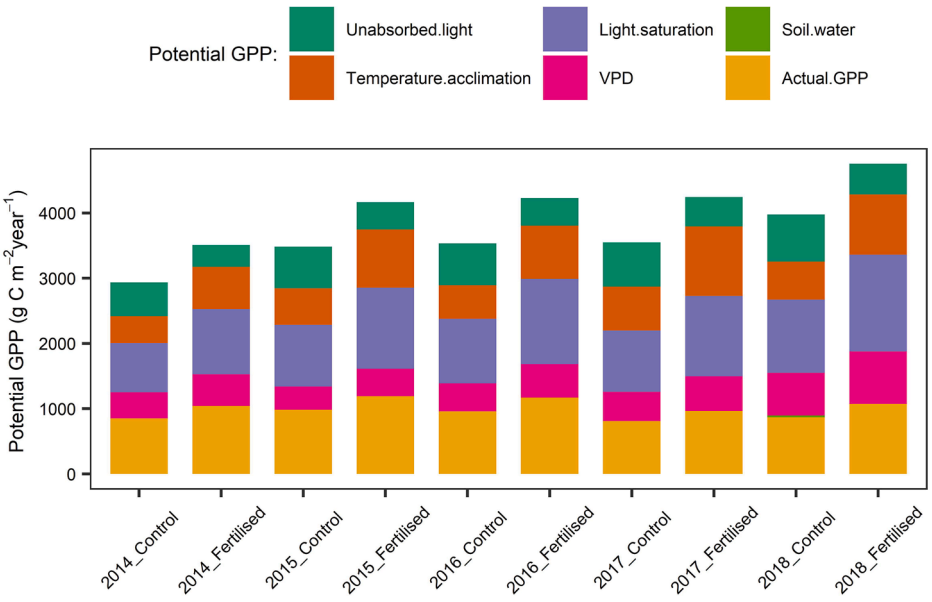

Fig. A6. Disaggregation of annual variation of potential production. GPP = gross primary production, VPD = vapour pressure deficit.

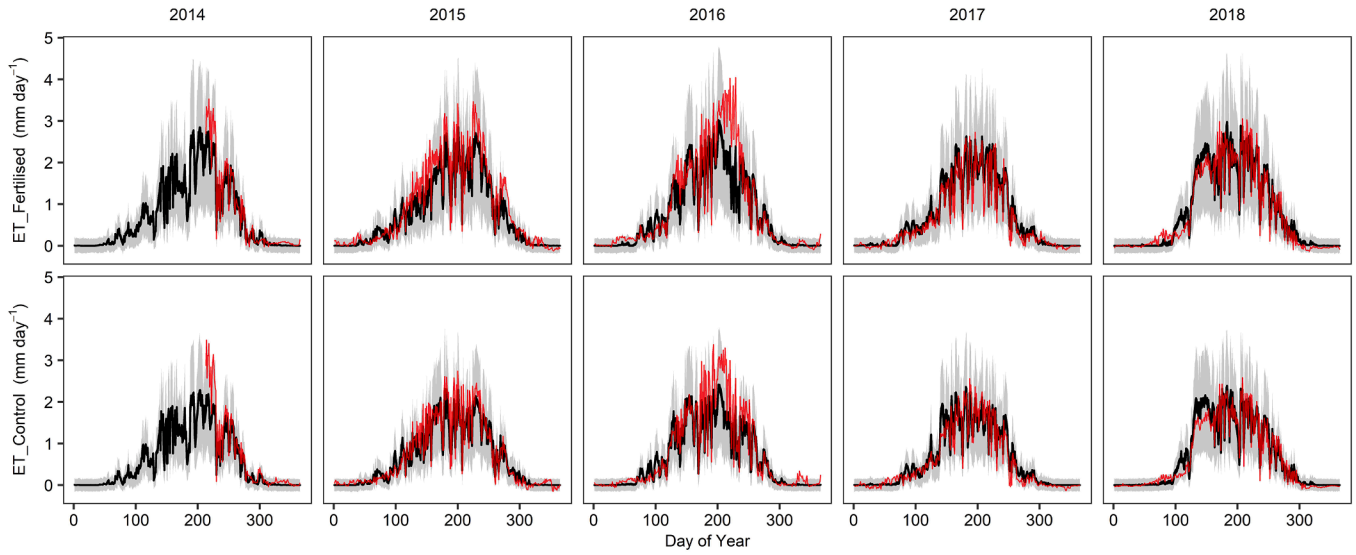

Fig. A7. Daily evapotranspiration. The red lines are eddy covariance observations without being filtered by the quality control flag. Black area is parametric uncertainty (negligible). Grey area is the predictive uncertainty that describes the possible ranges of the mismatches between PRELES and eddy covariance measurements. The uncertainty was qualified as 95% Bayesian credible intervals. ET = evapotranspiration.

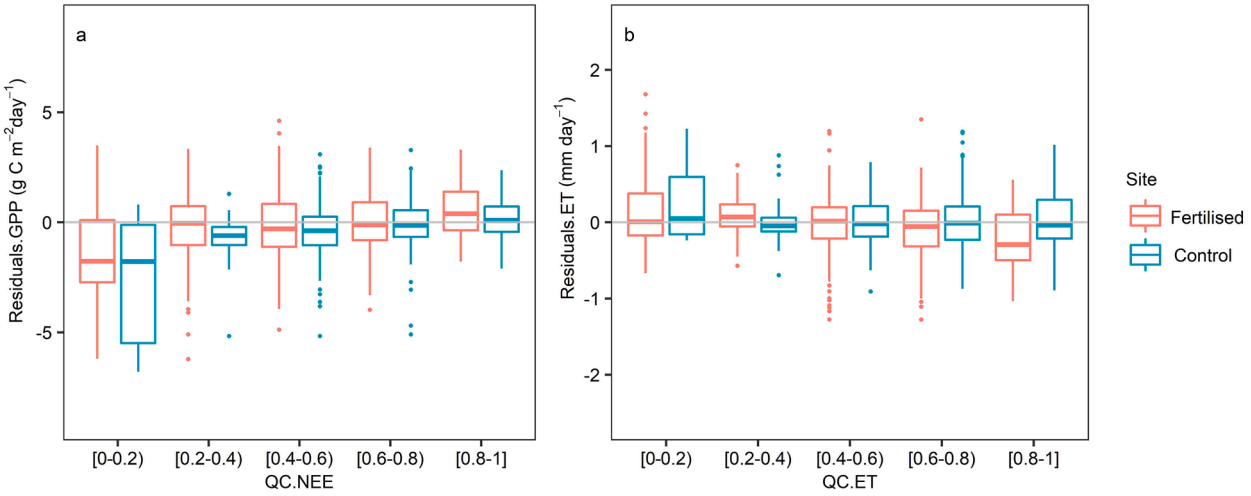

Fig. A8. Residuals over data quality of eddy covariance measurements. Residuals were calculated based on a 5-fold cross validation. The quality control flag, QC, varies between 0-1, indicating the percentage of measured half-hourly data used to calculate daily value. GPP = gross primary production, ET = evapotranspiration, NEE=net ecosystem exchange.

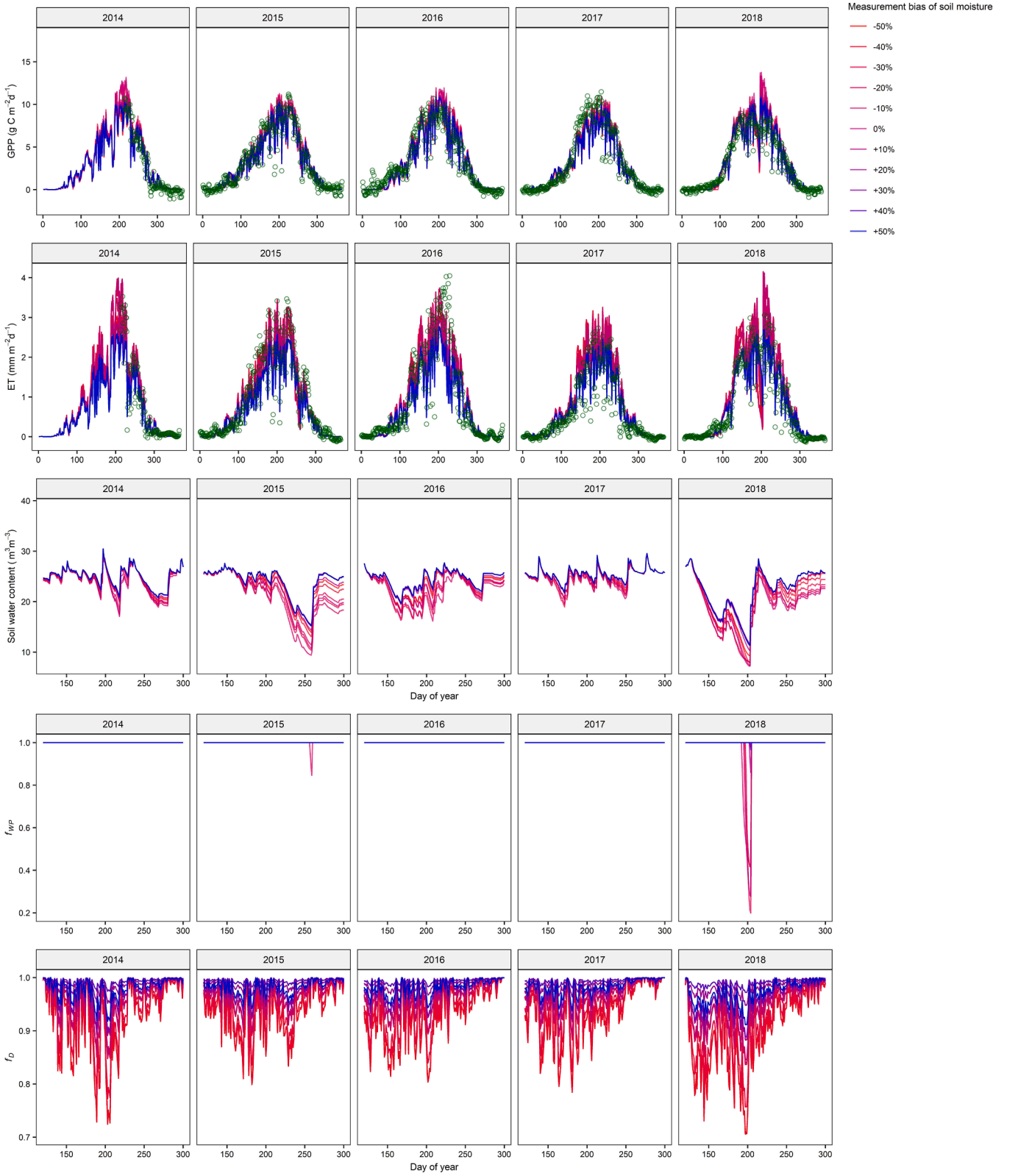

Fig. A9. A sensitivity analysis of the relationship between the model calibration and the error of soil moisture data. Green circles represent the eddy covariance measurements. Lines represent PRELES simulations when adding different biases to soil moisture data in model calibrations. GPP = gross primary production; ET = evapotranspiration; f_{wp} = modifier of soil water availability on GPP; f_D = modifier of vapour pressure deficit on GPP.

References

Andersson, C., Alpfjord Wylde, H., Engardt, M, 2018. Long-term sulfur and nitrogen deposition in Sweden: 1983-2013 reanalysis (Meteorology, No. 163). Swedish Meteorol. Hydrol. Inst. (SMHI).

Aubin, I., Beaudet, M., Messier, C., 2000. Light extinction coefficients specific to the understory vegetation of the southern boreal forest, Quebec. Can. J. For. Res. 30 (1), 168–177.

Aubinet, M., Vesala, T., Papale, D., 2012. Eddy covariance: a practical guide to measurement and data analysis. Springer Science & Business Media.

Bedison, J.E., McNeil, B.E., 2009. Is the growth of temperate forest trees enhanced along an ambient nitrogen deposition gradient? Ecology 90 (7), 1736–1742.

Beier, C., Beierkuhnlein, C., Wohlgemuth, T., Penuelas, J., Emmett, B., Körner, C., de Boeck, H., Christensen, J.H., Leuzinger, S., Janssens, I.A., Hansen, K., 2012. Precipitation manipulation experiments–challenges and recommendations for the future. Ecol. Lett. 15 (8), 899–911.

Betson, N.R., Johannisson, C., Löfvenius, M.O., Grip, H., Granström, A., Högberg, P., 2007. Variation in the δ13C of foliage of *Pinus sylvestris* L. in relation to climate and additions of nitrogen: analysis of a 32-year chronology. Glob. Change Biol. 13 (11), 2317–2328.

Bobbink, R., Hicks, K., Galloway, J., Spranger, T., Alkemade, R., Ashmore, M., Bustamante, M., Cinderby, S., Davidson, E., Dentener, F., Emmett, B., 2010. Global assessment of nitrogen deposition effects on terrestrial plant diversity: a synthesis. Ecol. Appl. 20 (1), 30–59.

Campbell, G.S., 1977. An introduction to environmental biophysics. Springer-Verlag, New York.

Chazdon, R.L., Pearcy, R.W., 1991. The importance of sunflecks for forest understory plants. Bioscience 41 (11), 760–766.

Cowan, I.R., Farquhar, G.D., 1977. Stomatal function in relation to leaf metabolism and environment. Symp. Soc. Exp. Biol. 31, 471.

De Bruin, H.A.R, 1981. The determination of (reference crop) evapotranspiration from routine weather data. Proceedings of Technical Meeting 38, Committee for Hydrological Research TNO, Evaporation in relation to hydrology. Proc. Inform. 28, 25–37.

Dezi, S., Medlyn, B.E., Tonon, G., Magnani, F., 2010. The effect of nitrogen deposition on forest carbon sequestration: a model-based analysis. Glob. Change Biol. 16 (5), 1470–1486.

Duursma, R.A., Kolari, P., Perämäki, M., Nikinmaa, E., Hari, P., Delzon, S., Loustau, D., Ilvesniemi, H., Pumpanen, J., Mäkelä, A., 2008. Predicting the decline in daily maximum transpiration rate of two pine stands during drought based on constant minimum leaf water potential and plant hydraulic conductance. Tree Physiol. 28 (2), 265–276.

Ellsworth, D.S., Reich, P.B., 1993. Canopy structure and vertical patterns of photosynthesis and related leaf traits in a deciduous forest. Oecologia 96 (2), 169–178.

Evans, J., 1989. Photosynthesis and nitrogen relationships in leaves of C3 plants. Oecologia 78, 9–19.

Ewers, B.E., Oren, R., Sperry, J.S., 2000. Root hydraulic conductance: a reflection of water balance and a constraint on canopy stomatal conductance. Plant Cell Environ. 23, 1055–1066.

Ewers, B.E., Oren, R., Phillips, N., Strömgren, M., Linder, S., 2001. Mean canopy stomatal conductance responses to water and nutrient availabilities in *Picea abies* and *Pinus taeda*. Tree Physiol. 21 (12–13), 841–850.

Fang, Y., Yoh, M., Koba, K., Zhu, W., Takebayashi, Y.U., Xiao, Y., Lei, C., Mo, J., Zhang, W.E.I., Lu, X., 2011. Nitrogen deposition and forest nitrogen cycling along an urban–rural transect in southern China. Glob. Change Biol. 17 (2), 872–885.

Ferwerda, J.G., Skidmore, A.K., 2007. Can nutrient status of four woody plant species be predicted using field spectrometry? ISPRS J. Photogram. Remote Sens. 62 (6), 406–414.

Field, C., Mooney, H., 1986. The photosynthesis-nitrogen relationship in wild plants. In: Givnish, T.J. (Ed.), On the Economy of Plant Form and Function. Cambridge University Press, Cambridge, pp. 25–55.

Fleischer, K., Rebel, K.T., Van Der Molen, M.K., Erisman, J.W., Wassen, M.J., Van Loon, E.E., Montagnani, L., Gough, C.M., Herbst, M., Janssens, I.A., Gianelle, D., 2013. The contribution of nitrogen deposition to the photosynthetic capacity of forests. Glob. Biogeochem. Cycles 27 (1), 187–199.

From, F., Strengbom, J., Nordin, A., 2015. Residual long-term effects of forest fertilization on tree growth and nitrogen turnover in boreal forest. Forests 6 (4), 1145–1156.

Gao, Y., Markkanen, T., Thum, T., Aurela, M., Lohila, A., Mammarella, I., Kämäräinen, M., Hagemann, S., Aalto, T., 2016. Assessing various drought indicators in representing summer drought in boreal forests in Finland. Hydrol. Earth Syst. Sci. 20, 175–191.

Gash, J.H.C., Culf, A.D., 1996. Applying a linear detrend to eddy correlation data in realtime. Bound.-Lay. Meteorol. 79 (3), 301–306.

Goulden, M.L., Crill, P.M., 1997. Automated measurements of CO_2 exchange at the moss surface of a black spruce forest. Tree Physiol. 17 (8–9), 537–542.

Hasselquist, N.J., Metcalfe, D.B., Marshall, J.D., Lucas, R.W., Högberg, P., 2016. Seasonality and nitrogen supply modify carbon partitioning in understory vegetation of a boreal coniferous forest. Ecology 97 (3), 671–683.

Haynes, B.E., Gower, S.T., 1995. Belowground carbon allocation in unfertilized and fertilized red pine plantations in northern Wisconsin. Tree Physiol. 15 (5), 317–325.

Jocher, G., De Simon, G., Hörnlund, T., Linder, S., Lundmark, T., Marshall, J., Nilsson, M. B., Näsholm, T., Tarvainen, L., Öquist, M., Peichl, M., 2017. Apparent winter CO_2 uptake by a boreal forest due to decoupling. Agricult. For. Meteorol. 232, 23–34.

Jocher, G., Marshall, J., Nilsson, M.B., Linder, S., De Simon, G., Hörnlund, T., Lundmark, T., Näsholm, T., Ottosson Löfvenius, M., Tarvainen, L., Wallin, G., 2018. Impact of canopy decoupling and subcanopy advection on the annual carbon balance of a boreal Scots pine forest as derived from eddy covariance. J. Geophys. Res. Biogeosci. 123 (2), 303–325.

Kergoat, L., Lafont, S., Arneth, A., Le Dantec, V., Saugier, B., 2008. Nitrogen controls plant canopy light-use efficiency in temperate and boreal ecosystems. J. Geophys. Res. Biogeosci. 113 (G4).

Kolari, P., Pumpanen, J., Kulmala, L., Ilvesniemi, H., Nikinmaa, E., Grönholm, T., Hari, P., 2006. Forest floor vegetation plays an important role in photosynthetic production of boreal forests. For. Ecol. Manage. 221 (1–3), 241–248.

Kull, O., Niinemets, Ü., 1998. Distribution of leaf photosynthetic properties in tree canopies: comparison of species with different shade tolerance. Funct. Ecol. 12 (3), 472–479.

Kulmala, L., Pumpanen, J., Hari, P., Vesala, T., 2009. Photosynthesis of boreal ground vegetation after a forest clear-cut. Biogeosciences 6, 2495–2507.

Kulmala, L., Pumpanen, J., Hari, P., Vesala, T., 2011. Photosynthesis of ground vegetation in different aged pine forests: Effect of environmental factors predicted with a process-based model. J. Veg. Sci. 22, 96–110.

Landsberg, J., Sands, P., 2011. Physiological ecology of forest production: principles, processes and models, Vol. 4. Elsevier/Academic Press, London.

Laudon, H., Taberman, I., Ågren, A., Futter, M., Ottosson-Löfvenius, M., Bishop, K., 2013. The Krycklan Catchment Study—A flagship infrastructure for hydrology, biogeochemistry, and climate research in the boreal landscape. Water Resour. Res. 49 (10), 7154–7158.

Leppälammi-Kujansuu, J., Salemaa, M., Kleja, D.B., Linder, S., Helmisaari, H.S., 2014. Fine root turnover and litter production of Norway spruce in a long-term temperature and nutrient manipulation experiment. Plant and Soil 374 (1-2), 73–88.

Lim, H., Oren, R., Palmroth, S., Tor-ngern, P., Mörling, T., Näsholm, T., Lundmark, T., Helmisaari, H.S., Leppälammi-Kujansuu, J., Linder, S., 2015. Inter-annual variability of precipitation constrains the production response of boreal *Pinus sylvestris* to nitrogen fertilization. For. Ecol. Manage. 348, 31–45.

Linder, S., Axelsson, B., 1982. Changes in carbon uptake and allocation patterns as a result of irrigation and fertilization in a young *Pinus sylvestris* stand. In: Waring, R.H. (Ed.), Carbon uptake and allocation in subalpine ecosystems as a key to management. Forest Research Laboratory, Oregon State University, Corvallis, U.S.A., pp. 38–44

Linder, S., Troeng, E., 1980. Photosynthesis and transpiration of 20-year-old Scots pine. Ecol. Bull. (Stockholm) 165–181.

Loozen, Y., Rebel, K.T., de Jong, S.M., Lu, M., Ollinger, S.V., Wassen, M.J., Karssenberg, D., 2020. Mapping canopy nitrogen in European forests using remote sensing and environmental variables with the random forests method. Rem. Sens. Environ. 247, 111933.

Magnani, F., Mencuccini, M., Borghetti, M., Berbigier, P., Berninger, F., Delzon, S., Grelle, A., Hari, P., Jarvis, P.G., Kolari, P., Kowalski, A.S., 2007. The human footprint in the carbon cycle of temperate and boreal forests. Nature 447 (7146), 849–851.

Martin, M.E., Aber, J.D., 1997. High spectral resolution remote sensing of forest canopy lignin, nitrogen, and ecosystem processes. Ecol. Appl. 7 (2), 431–443.

Martin, M.E., Plourde, L.C., Ollinger, S.V., Smith, M.L., McNeil, B.E., 2008. A generalizable method for remote sensing of canopy nitrogen across a wide range of forest ecosystems. Rem. Sens. Environ. 112 (9), 3511–3519.

Mauder, M., Foken, T., 2004. Documentation and instruction manual of the eddy-covariance software package TK2 1–67.

Mäkelä, A., Pulkkinen, M., Kolari, P., Lagergren, F., Berbigier, P., Lindroth, A., Loustau, D., Nikinmaa, E., Vesala, T., Hari, P., 2008. Developing an empirical model of stand GPP with the LUE approach: analysis of eddy covariance data at five contrasting conifer sites in Europe. Glob. Change Biol. 14 (1), 92–108.

McMahon, T.A., Peel, M.C., Lowe, L., Srikanthan, R., McVicar, T.R., 2012. Estimating actual, potential, reference crop and pan evaporation using standard meteorological data: a pragmatic synthesis. Hydrol. Earth Syst. Sci. Discuss. 9 (10).

Mellander, P.E., Laudon, H., Bishop, K., 2005. Modelling variability of snow depths and soil temperatures in Scots pine stands. Agricult. For. Meteorol. 133 (1–4), 109–118.

McAdam, S.A., Brodribb, T.J., 2015. The evolution of mechanisms driving the stomatal response to vapor pressure deficit. Plant Physiol. 167 (3), 833–843.

Middleton, N.J., Thomas, D.S.G., 1992. UNEP: world atlas of desertification. Edward Arnold, Sevenoaks.

Minunno, F., Peltoniemi, M., Launiainen, S., Aurela, M., Lindroth, A., Lohila, A., Mammarella, I., Minkkinen, K., Mäkelä, A., 2016. Calibration and validation of a semi-empirical flux ecosystem model for coniferous forests in the boreal region. Ecol. Model. 341, 37–52.

Misson, L., Baldocchi, D.D., Black, T.A., Blanken, P.D., Brunet, Y., Yuste, J.C., Dorsey, J. R., Falk, M., Granier, A., Irvine, M.R., Jarosz, N., 2007. Partitioning forest carbon fluxes with overstory and understory eddy-covariance measurements: A synthesis based on FLUXNET data. Agricult. For. Meteorol. 144 (1–2), 14–31.

Moffat, A.M., Papale, D., Reichstein, M., Hollinger, D.Y., Richardson, A.D., Barr, A.G., Beckstein, C., Braswell, B.H., Churkina, G., Desai, A.R., Falge, E., 2007. Comprehensive comparison of gap-filling techniques for eddy covariance net carbon fluxes. Agricult. For. Meteorol. 147 (3–4), 209–232.

Morén, A.S., Lindroth, A., 2000. CO_2 exchange at the floor of a boreal forest. Agricult. For. Meteorol. 101 (1), 1–14.

Nilsson, L.O., Wallander, H., 2003. Production of external mycelium by ectomycorrhizal fungi in a Norway spruce forest was reduced in response to nitrogen fertilization. New Phytol. 158 (2), 409–416.

Nohrstedt, H.Ö., 2001. Response of coniferous forest ecosystems on mineral soils to nutrient additions: a review of Swedish experiences. Scand. J. For. Res. 16 (6), 555–573.

Nordin, A., Näsholm, T., Ericson, L., 1998. Effects of simulated N deposition on understorey vegetation of a boreal coniferous forest. Funct. Ecol. 12 (4), 691–699.
Novick, K.A., Ficklin, D.L., Stoy, P.C., Williams, C.A., Bohrer, G., Oishi, A.C., Papuga, S. A., Blanken, P.D., Noormets, A., Sulman, B.N., Scott, R.L., 2016. The increasing importance of atmospheric demand for ecosystem water and carbon fluxes. Nat. Clim. Change 6 (11), 1023–1027.
Nömmik, H., Vahtras, K., 1982. Retention and fixation of ammonium and ammonia in soils. Nitrogen in agricultural soils. Nitrogeninagrics 123–171.
Oren, R., Sperry, J.S., Katul, G.G., Pataki, D.E., Ewers, B.E., Phillips, N., Schäfer, K.V.R., 1999. Survey and synthesis of intra-and interspecific variation in stomatal sensitivity to vapour pressure deficit. Plant Cell Environ. 22 (12), 1515–1526.
Palmroth, S., Bach, L.H., Nordin, A., Palmqvist, K., 2014. Nitrogen-addition effects on leaf traits and photosynthetic carbon gain of boreal forest understory shrubs. Oecologia 175 (2), 457–470.
Papale, D., Reichstein, M., Aubinet, M., Canfora, E., Bernhofer, C., Kutsch, W., Longdoz, B., Rambal, S., Valentini, R., Vesala, T., Yakir, D., 2006. Towards a standardized processing of Net Ecosystem Exchange measured with eddy covariance technique: algorithms and uncertainty estimation. Biogeosciences 3 (4), 571–583.
Paul-Limoges, E., Wolf, S., Eugster, W., Hörtnagl, L., Buchmann, N., 2017. Below-canopy contributions to ecosystem CO_2 fluxes in a temperate mixed forest in Switzerland. Agricult. For. Meteorol. 247, 582–596.
Peltoniemi, M., Pulkkinen, M., Kolari, P., Duursma, R.A., Montagnani, L., Wharton, S., Lagergren, F., Takagi, K., Verbeeck, H., Christensen, T., Vesala, T., 2012a. Does canopy mean nitrogen concentration explain variation in canopy light use efficiency across 14 contrasting forest sites? Tree Physiol. 32 (2), 200–218.
Peltoniemi, M., Duursma, R.A., Medlyn, B.E., 2012b. Co-optimal distribution of leaf nitrogen and hydraulic conductance in plant canopies. Tree Physiol. 32 (5), 510–519.
Peltoniemi, M., Pulkkinen, M., Aurela, M., Pumpanen, J., Kolari, P., Mäkelä, A, 2015. A semi-empirical model of boreal-forest gross primary production, evapotranspiration, and soil water — calibration and sensitivity analysis. Boreal Environ. Res. 20, 151–171.
Phil-Karlsson, G., Akselsson, C., Hellsten, S., Karlsson, P.E., Malm, G., 2009. Övervakning av luftföroreningar i norra Sverige—mätningar och modellering. Svenska Miljöinstitutet, Stockholm.
Potter, C.S., Randerson, J.T., Field, C.B., Matson, P.A., Vitousek, P.M., Mooney, H.A., Klooster, S.A., 1993. Terrestrial ecosystem production: a process model based on global satellite and surface data. Glob. Biogeochem. Cycles 7 (4), 811–841.
Reichstein, M., Falge, E., Baldocchi, D., Papale, D., Aubinet, M., Berbigier, P., Bernhofer, C., Buchmann, N., Gilmanov, T., Granier, A., Grünwald, T., 2005. On the separation of net ecosystem exchange into assimilation and ecosystem respiration: review and improved algorithm. Glob. Change Biol. 11 (9), 1424–1439.
Reich, P.B., Walters, M.B., Kloeppel, B.D., Ellsworth, D.S., 1995. Different photosynthesis-nitrogen relations in deciduous hardwood and evergreen coniferous tree species. Oecologia 104 (1), 24–30.
Reich, P.B., Walters, M.B., Ellsworth, D.S., 1997. From tropics to tundra: global convergence in plant functioning. Proc. Natl. Acad. Sci. 94 (25), 13730–13734.
Rustad, L.E.J.L., Campbell, J., Marion, G., Norby, R., Mitchell, M., Hartley, A., Cornelissen, J., Gurevitch, J., 2001. A meta-analysis of the response of soil respiration, net nitrogen mineralization, and aboveground plant growth to experimental ecosystem warming. Oecologia 126 (4), 543–562.
Schiestl-Aalto, P., Kulmala, L., Mäkinen, H., Nikinmaa, E., Mäkelä, A., 2015. CASSIA–a dynamic model for predicting intra-annual sink demand and interannual growth variation in S cots pine. New Phytol. 206 (2), 647–659.
Schwalm, C.R., Black, T.A., Amiro, B.D., Arain, M.A., Barr, A.G., Bourque, C.P.A., Dunn, A.L., Flanagan, L.B., Giasson, M.A., Lafleur, P.M., Margolis, H.A., 2006. Photosynthetic light use efficiency of three biomes across an east–west continental-scale transect in Canada. Agricult. For. Meteorol. 140 (1–4), 269–286.
Simmons, A.J., Willett, K.M., Jones, P.D., Thorne, P.W., Dee, D.P., 2010. Low-frequency variations in surface atmospheric humidity, temperature, and precipitation: Inferences from reanalyses and monthly gridded observational data sets. J. Geophys. Res. Atmos. 115 (D1).
Sims, D.A., Rahman, A.F., Cordova, V.D., El-Masri, B.Z., Baldocchi, D.D., Bolstad, P.V., Flanagan, L.B., Goldstein, A.H., Hollinger, D.Y., Misson, L., Monson, R.K., 2008. A new model of gross primary productivity for North American ecosystems based solely on the enhanced vegetation index and land surface temperature from MODIS. Rem. Sens. Environ. 112 (4), 1633–1646.
Sivia, D., Skilling, J., 2006. Data analysis: a Bayesian tutorial. OUP, Oxford.
Smith, F.W., Sampson, D.A., Long, J.N., 1991. Comparison of leaf area index estimates from tree allometrics and measured light interception. For. Sci. 37 (6), 1682–1688.
Stein, B.R., Thomas, V.A., Lorentz, L.J., Strahm, B.D., 2014. Predicting macronutrient concentrations from loblolly pine leaf reflectance across local and regional scales. GISci. Rem. Sens. 51 (3), 269–287.
Stenberg, P., Linder, S., Smolander, H., 1995. Variation in the ratio of shoot silhouette area to needle area in fertilized and unfertilized Norway spruce trees. Tree Physiol. 15 (11), 705–712.
Stenberg, P., Kangas, T., Smolander, H., Linder, S., 1999. Shoot structure, canopy openness, and light interception in Norway spruce. Plant Cell Environ. 22 (9), 1133–1142.
Tamm, C.O., 1991. Nitrogen in Terrestrial Ecosystems. Questions of Productivity, Vegetational Changes, and Ecosystem Stability. Ecol. Stud. 81, 115. ISBN 3-540-51807-X.
Tang, Z., Chambers, J.L., Guddanti, S., Barmett, J.P., 1999. Thinning, fertilization, and crown position interact to control physiological responses of loblolly pine. Tree Physiol. 19 (2), 87–94.
Tarvainen, L., Lutz, M., Räntfors, M., Näsholm, T., Wallin, G., 2016. Increased needle nitrogen contents did not improve shoot photosynthetic performance of mature nitrogen-poor Scots pine trees. Front. Plant Sci. 7, 1051.
Thomas, J.R., Oerther, G.F., 1972. Estimating nitrogen content of sweet pepper leaves by reflectance measurements 1. Agron. J. 64 (1), 11–13.
Thornthwaite, C.W., 1948. An approach toward a rational classification of climate. Geograph. Rev. 38 (1), 55–94.
Tian, X., Minunno, F., Cao, T., Peltoniemi, M., Kalliokoski, T., Mäkelä, A., 2020. Extending the range of applicability of the semi-empirical ecosystem flux model PRELES for varying forest types and climate. Glob. Change Biol. 26 (5), 2923–2943.
Turner, D.P., Urbanski, S., Bremer, D., Wofsy, S.C., Meyers, T., Gower, S.T., Gregory, M., 2003. A cross-biome comparison of daily light use efficiency for gross primary production. Glob. Change Biol. 9 (3), 383–395.
Vitousek, P.M., Howarth, R.W., 1991. Nitrogen limitation on land and in the sea: how can it occur? Biogeochemistry 13 (2), 87–115.
Wang, Z., Wang, T., Darvishzadeh, R., Skidmore, A.K., Jones, S., Suarez, L., Woodgate, W., Heiden, U., Heurich, M., Hearne, J., 2016. Vegetation indices for mapping canopy foliar nitrogen in a mixed temperate forest. Rem. Sens. 8 (6), 491.
Watt, M.S., Pearse, G.D., Dash, J.P., Melia, N., Leonardo, E.M.C., 2019. Application of remote sensing technologies to identify impacts of nutritional deficiencies on forests. ISPRS J. Photogram. Rem. Sens. 149, 226–241.
Wilczak, J.M., Oncley, S.P., Stage, S.A., 2001. Sonic anemometer tilt correction algorithms. Bound.-Lay. Meteorol. 99 (1), 127–150.
Willett, K.M., Dunn, R.J.H., Thorne, P.W., Bell, S., De Podesta, M., Parker, D.E., Jones, P. D., Williams Jr, C.N., 2014. HadISDH land surface multi-variable humidity and temperature record for climate monitoring. Clim. Past 10 (6), 1983–2006.
Wright, I.J., Reich, P.B., Westoby, M., Ackerly, D.D., Baruch, Z., Bongers, F., Cavender-Bares, J., Chapin, T., Cornelissen, J.H., Diemer, M., Flexas, J., 2004. The worldwide leaf economics spectrum. Nature 428 (6985), 821–827.
Wutzler, T., Lucas-Moffat, A., Migliavacca, M., Knauer, J., Sickel, K., Šigut, L., Menzer, O., Reichstein, M., 2018. Basic and extensible post-processing of eddy covariance flux data with REddyProc. Biogeosciences 15 (16), 5015–5030.
Yuan, W., Liu, S., Zhou, G., Zhou, G., Tieszen, L.L., Baldocchi, D., Bernhofer, C., Gholz, H., Goldstein, A.H., Goulden, M.L., Hollinger, D.Y., 2007. Deriving a light use efficiency model from eddy covariance flux data for predicting daily gross primary production across biomes. Agricult. For. Meteorol. 143 (3–4), 189–207.
Yuan, W., Cai, W., Xia, J., Chen, J., Liu, S., Dong, W., Merbold, L., Law, B., Arain, A., Beringer, J., Bernhofer, C., 2014. Global comparison of light use efficiency models for simulating terrestrial vegetation gross primary production based on the LaThuile database. Agricult. For. Meteorol. 192, 108–120.
Yuan, W., Zheng, Y., Piao, S., Ciais, P., Lombardozzi, D., Wang, Y., Ryu, Y., Chen, G., Dong, W., Hu, Z., Jain, A.K., 2019. Increased atmospheric vapor pressure deficit reduces global vegetation growth. Sci. Adv. 5 (8), 1396.
Zheng, Y., Zhang, L., Xiao, J., Yuan, W., Yan, M., Li, T., Zhang, Z., 2018. Sources of uncertainty in gross primary productivity simulated by light use efficiency models: Model structure, parameters, input data, and spatial resolution. Agricult. For. Meteorol. 263, 242–257.